AGU PUBLICATIONS

JGR

Journal of Geophysical Research: Solid Earth

RESEARCH ARTICLE
10.1002/2014JB011617

Key Points:
- Three-dimensional acoustic water column surveys conducted in the Sea of Marmara
- No gas emissions along the Istanbul-Silivri and Princes Islands seismic gaps
- Spatiotemporal gas emission distribution may constrain earthquake geohazards

Correspondence to:
S. Dupré,
stephanie.dupre@ifremer.fr

Citation:
Dupré, S., C. Scalabrin, C. Grall, J.-M. Augustin, P. Henry, A. M. C. Şengör, N. Görür, M. N. Çağatay, and L. Géli (2015), Tectonic and sedimentary controls on widespread gas emissions in the Sea of Marmara: Results from systematic, shipborne multibeam echo sounder water column imaging, *J. Geophys. Res. Solid Earth*, *120*, 2891–2912, doi:10.1002/2014JB011617.

Received 19 SEP 2014
Accepted 11 APR 2015
Accepted article online 15 APR 2015
Published online 18 MAY 2015

Tectonic and sedimentary controls on widespread gas emissions in the Sea of Marmara: Results from systematic, shipborne multibeam echo sounder water column imaging

Stéphanie Dupré[1], Carla Scalabrin[1], Céline Grall[1,2], Jean-Marie Augustin[1], Pierre Henry[2], A. M. Celal Şengör[3], Naci Görür[3], M. Namık Çağatay[3], and Louis Géli[1]

[1]IFREMER, Marine Geosciences, Plouzané, France, [2]CEREGE, CNRS, Université Aix Marseille, Marseille, France, [3]Istanbul Technical University, Faculty of Mining, Istanbul, Turkey

Abstract Understanding of the evolution of fluid-fault interactions during earthquake cycles is a challenge that acoustic gas emission studies can contribute. A survey of the Sea of Marmara using a shipborne, multibeam echo sounder, with water column records, provided an accurate spatial distribution of offshore seeps. Gas emissions are spatially controlled by a combination of factors, including fault and fracture networks in connection to the Main Marmara Fault system and inherited faults, the nature and thickness of sediments (e.g., occurrence of impermeable or gas-bearing sediments and landslides), and the connectivity between the seafloor and gas sources, particularly in relation to the Eocene Thrace Basin. The relationship between seepage and fault activity is not linear, as active faults do not necessarily conduct gas, and scarps corresponding to deactivated fault strands may continue to channel fluids. Within sedimentary basins, gas is not expelled at the seafloor unless faulting, deformation, or erosional processes affect the sediments. On topographic highs, gas flares occur along the main fault scarps but are also associated with sediment deformation. The occurrence of gas emissions appears to be correlated with the distribution of microseismicity. The relative absence of earthquake-induced ground shaking along parts of the Istanbul-Silivri and Princes Islands segments is likely the primary factor responsible for the comparative lack of gas emissions along these fault segments. The spatiotemporal distribution of gas seeps may thus provide a complementary way to constrain earthquake geohazards by focusing the study on some key fault segments, e.g., the northern part of the locked Princes Islands segment.

1. Introduction

The observation of cold seeps in association with active submarine faults [*Deville et al.*, 2003; *Henry et al.*, 2002; *Le Pichon et al.*, 1992; *Moore et al.*, 1990] suggests that at least some of these faults could channel fluids within the sediments from deep levels and, possibly, from the seismogenic zone in the crust. This hypothesis has been proposed for the submerged section of the North Anatolian Fault system within the Sea of Marmara, which is characterized by an intense seismic and fluid emission activity at the seabed. The seismic activity in the Sea of Marmara region over the past 500 years included numerous catastrophic earthquakes characterized by shallow focal depths of the seismic events ($<$20 km) [*Sato et al.*, 2004]. During the twentieth century, there were five earthquakes with a magnitude >7 [*Ambraseys and Jackson*, 2000] (Figure 1). The understanding of the fluid-fault coupling processes is a challenge of critical importance and addresses fundamental questions, such as the variation of the physical and chemical properties of the fluids within the fault zone during an earthquake cycle.

The use of acoustic techniques to detect gas emissions escaping through the seabed into the water column has dramatically increased in recent years, providing new insights into the processes involving coupling between the fluid and tectonic activity. The water column above the submerged section of the North Anatolian Fault within the Marmara Sea was investigated in 2000 and 2007 using side-scan and single-beam sonars along a few unevenly distributed profiles [*Géli et al.*, 2008]. Most gas emissions in the water column were found near the surface expression of known active faults during these earlier surveys. However, the effect of a possible bias related to the fact that most profiles were purposely implemented along active faults still needed to be investigated. A systematic survey of the deepest areas of the Sea of Marmara ($>$300 m) was thus conducted

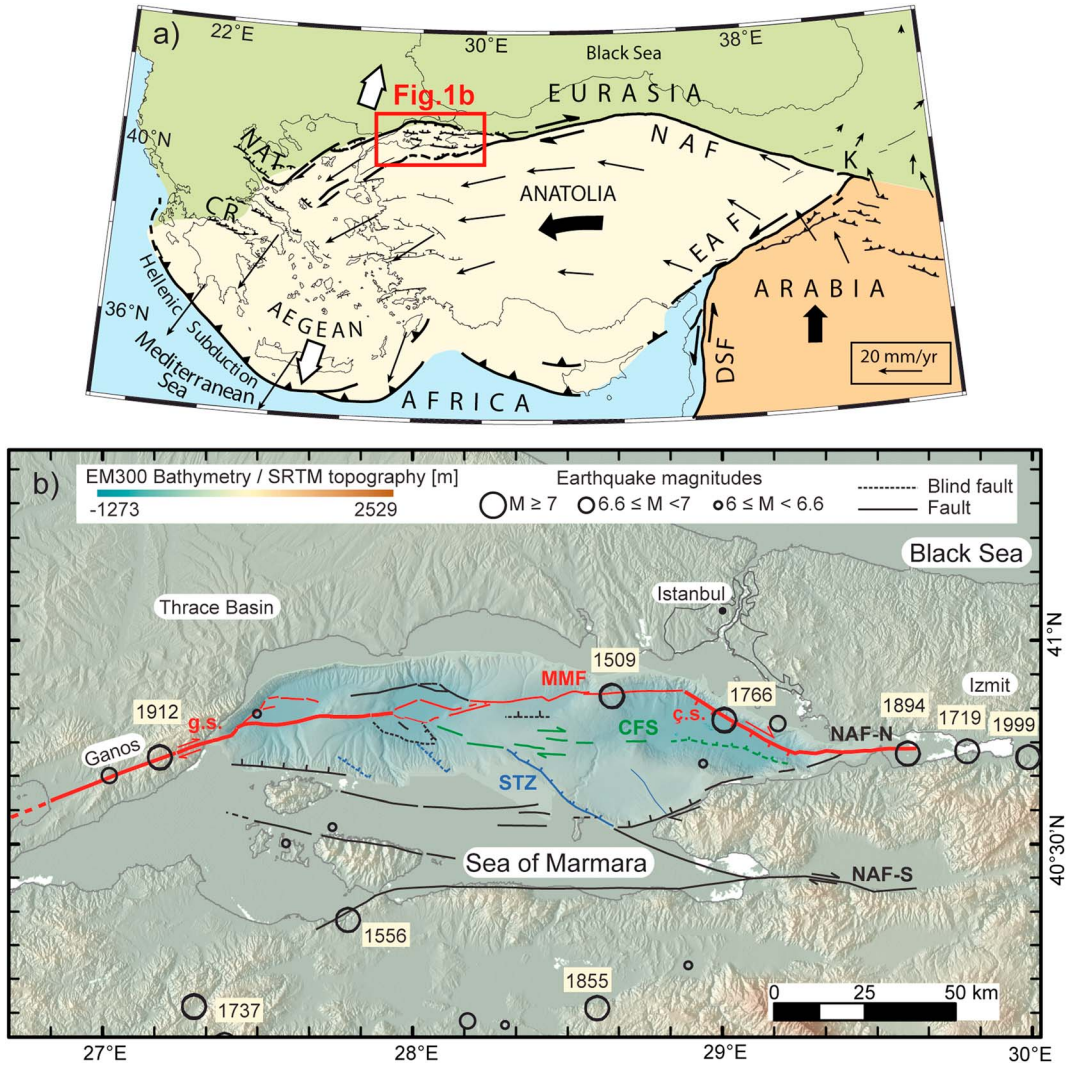

Figure 1. (a) Tectonic setting of continental extrusion in the eastern Mediterranean from *Armijo et al.* [1999]. The current motion of the Anatolian and Arabian plates with respect to Eurasia are reported with GPS (Global Positioning System) and SLR (Satellite Laser Ranging) velocity vectors in mm/yr from *Reilinger et al.* [1997]. NAF, North Anatolian Fault; EAF, East Anatolian Fault; K, Karliova triple junction; DSF, Dead Sea Fault; NAT, North Aegean Trough; CR, Corinth Rift. (b) Structural map of the Sea of Marmara region with the fault network compiled by *Grall et al.* [2012]. NAF-N and NAF-S are the northern and southern segments of the North Anatolian Fault, respectively [*Seeber et al.*, 2006]. Red is the Main Marmara Fault (MMF) [*Le Pichon et al.*, 2001]. Red thick lines are the two main segments of the MMF: the Ganos segment (g.s.) and the Çınarcık segment (ç.s.). Blue is the South Transtensional Zone (STZ). Green is the Central Fault System (CFS). The fault system on the southern shelf is from *Parke et al.* [1999]. Large black circles are major earthquakes with a magnitude of 7 and above [*Ambraseys and Jackson*, 2000]. Bathymetry data were acquired with a Kongsberg EM300 multibeam echo sounder during the Marmara expedition in 2000 [*Le Pichon et al.*, 2001; *Rangin et al.*, 2001]. Topography data are from the 2000 Shuttle Radar Topography Mission.

in 2009 using a shipborne, multibeam echo sounder Kongsberg EM302, in order to establish an accurate spatial distribution of the seeps at the scale of the entire sea and to investigate the factors that control this distribution. The results of this survey are presented in this paper.

2. Geological Setting

2.1. Structural Setting and Seismic Activity

The highly active right-lateral strike-slip North Anatolian Fault (NAF) separates the Anatolian Scholle [*Dewey and Şengör*, 1979] from Eurasia and is more than 1200 km long [*Ketin*, 1948; *Şengör et al.*, 2005] (Figure 1a). The kinematics involves a westward displacement and a counterclockwise rotation of the

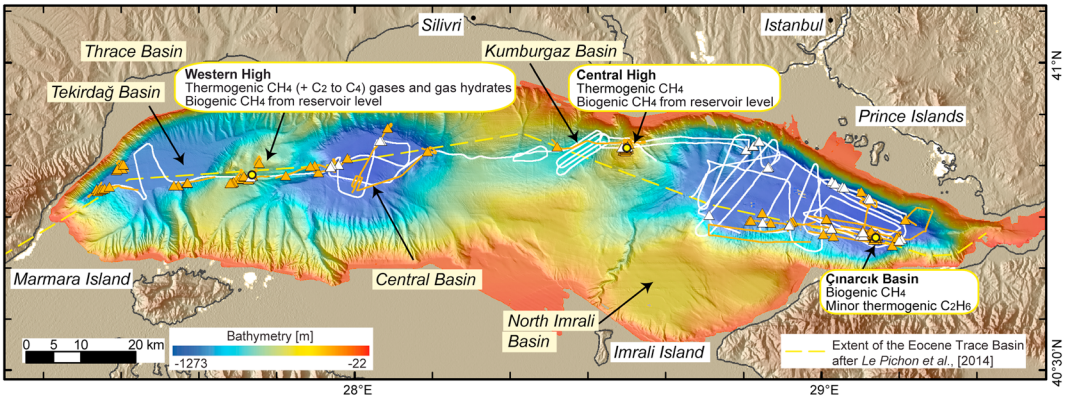

Figure 2. Acoustic gas escape distribution in the Sea of Marmara prior to 2009 [*Géli et al*., 2008]. White triangles stand for acoustic anomalies detected in September 2000 (Marmara expedition) and recorded in the water column of the raw side-scan-sonar data (SAR, 180 kHz). Orange triangles indicate the locations of acoustic anomalies detected in May–June 2007 (Marnaut expedition) using the sea-surface-towed echo sounder EK60 sonar (38 kHz). Track lines for each tool are reported to indicate coverage. Yellow dots refer to in situ gas and gas hydrates samples with indications of the gas origin [*Bourry et al*., 2009; *Ruffine et al*., 2012]. At the Western and Central highs, the biogenic methane is generated at the reservoir level, resulting from the biodegradation of oil and methanogenesis [*Ruffine et al*., 2012], unlike the biogenic methane at the Çınarcık Basin. The offshore extent of the Eocene Thrace Basin from *Le Pichon et al*. [2014] is indicated (dotted yellow line).

Anatolian Scholle with respect to Eurasia. Slip rates derived from GPS studies reach more than 20 mm/yr [*McClusky et al*., 2000; *Reilinger et al*., 1997; *Şengör et al*., 2005] and are similar to the ones derived from long-term plate tectonic reconstructions [*Armijo et al*., 1999; *Le Pichon et al*., 2001; *Şengör et al*., 2005]; this rate has been reached only in the last several hundred thousand years within the area under investigation in this paper [*Grall et al*., 2013; *Şengör et al*., 2005, 2014]. Most of the present-day slip motion is concentrated along the northern branch of the NAF (labeled NAF-N in Figure 1b), across the Sea of Marmara [*Armijo et al*., 1999; *Ergintav et al*., 2014; *McClusky et al*., 2000]. The Sea of Marmara lies between two strike-slip faults that both ruptured during the 7.4 magnitude Ganos (1912) and Izmit (1999) earthquakes, east and west, respectively (Figure 1b) [*Aksoy et al*., 2010; *Ambraseys and Finkel*, 1987; *Barka et al*., 2002; *Şengör et al*., 2005]. The Sea of Marmara, a complex set of basins of diverse, strike-slip-related origin, superimposed on a medial Miocene rift is bordered to the northwest by the Eocene Thrace Basin (Figures 1b and 2), which began developing as a fore-arc basin but became a postcollisional intermontane basin after the earliest Oligocene period, at the latest [*Görür and Elbek*, 2013; *Şengör et al*., 2005, 2014]. The Sea of Marmara resulted from the development of the North Anatolian Shear Zone during the late Pliocene to Pleistocene along a variety of Riedel, anti-Riedel, and P shears of the postpeak and preresidual structural stages [*Görür and Elbek*, 2013; *Şengör et al*., 2005, 2014]. The Sea of Marmara is crossed by a set of faults belonging to the northern branch of the NAF with major normal faults along both the northern and southern margins, dipping south and north, respectively [*Parke et al*., 1999], plus a recently discovered and partly active major strike-slip fault, namely, the South Marmara Fault [*Le Pichon et al*., 2014]. Several deep subbasins form the Sea of Marmara, from east to west, the Çınarcık, Kumburgaz, Central and Tekirdağ basins separated by two major bathymetric highs, the Central and Western highs (Figures 1b and 2) [*Le Pichon et al*., 2001; *Rangin et al*., 2001; *Şengör et al*., 2005, 2014]. Water depths range from 1100 to 1270 m in the deepest parts of the Sea of Marmara, with an average water depth of ~600 m on the bathymetric highs.

2.2. Cold Seeps and Active Faulting

The understanding of the evolution of the fluid-fault coupling processes during an earthquake cycle is a challenge, and the acoustic detection of gas emissions through the seabed may provide new insights on these processes [see, e.g., *Bayrakci et al*., 2014; *Gasperini et al*., 2012]. Fluid escape may occur both offshore and onshore [*Capozzi and Picotti*, 2002; *Delisle et al*., 2002; *Judd and Hovland*, 2007] at the seabed or terrestrial surface to give birth to seep-related structures, e.g., mud volcanoes [*Kopf*, 2002] resulting from the mobilization of gas (predominantly methane), water, and mud at a subbottom depth of a few meters

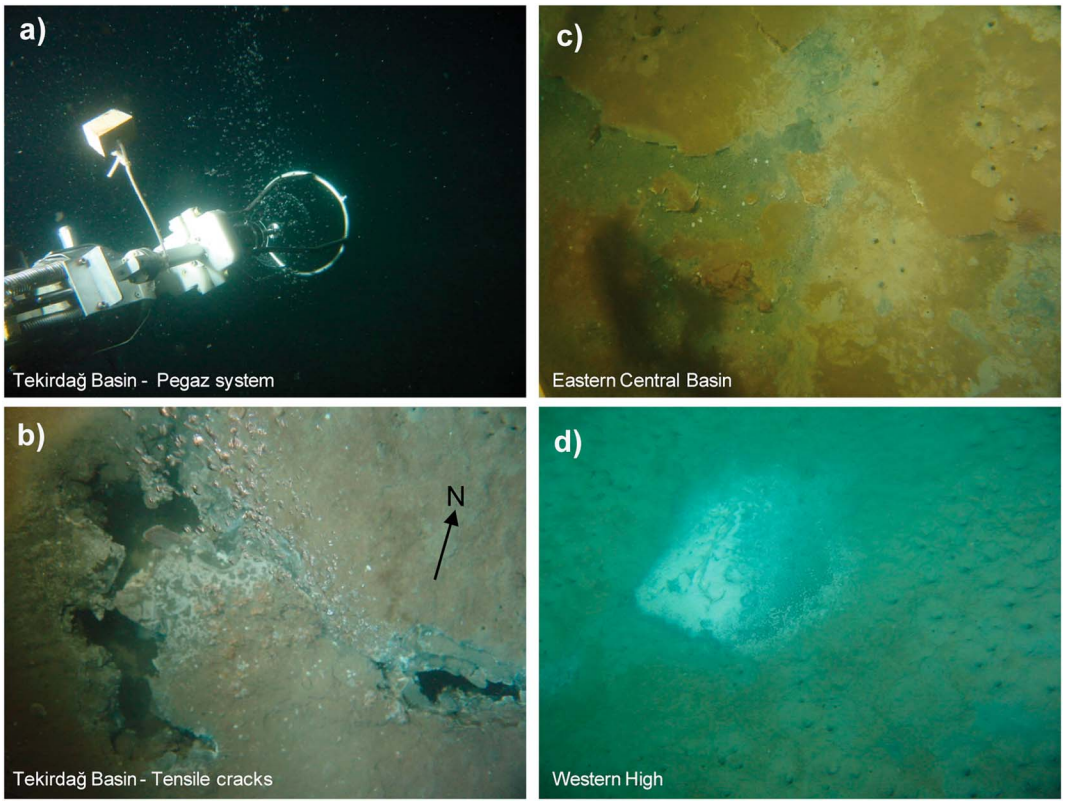

Figure 3. Seabed pictures acquired onboard the *Nautile* submersible during the Marnaut expedition in 2007 (© Ifremer). (a) String of gas bubbles along the northern escarpment of the Tekirdağ Basin. The Ifremer Pegaz system is dedicated to the in situ collection of fluids under pressure. (b) Tensile cracks associated with spontaneous gas emissions along the same escarpment. (c) Reduced dark sediments, most likely indicators of AOM occurrence, surrounded by holes created by gas expulsion through the seabed. Note the difference in sediment color due to the redeposition of suspended particles during fluid expulsion events (eastern edge of the Central Basin). (d) Active seeps associated with gas-saturated sediments at the Western High. The dark reduced sediment patch is partially covered, most presumably with bacterial mats.

to kilometers [*Dupré et al.*, 2014b]. Seabed fluid seepage commonly occurs at continental margins. The occurrence of seeps and the tectonic control on gas escape through the seabed have been the subject of numerous studies in a variety of environments, e.g., the West African Basins [*Gay et al.*, 2007], the Nile Deep Sea Fan [*Dupré et al.*, 2010; *Loncke et al.*, 2004], and the Eastern Mediterranean Anaximander Mountains [*Zitter et al.*, 2006]. Earthquakes trigger gas seeps that have been documented in a number of cases, including gas release at mud volcanoes [*Delisle et al.*, 2002; *Mellors et al.*, 2007; *Rudolph and Manga*, 2010; *Tsunogai et al.*, 2012]. *Field and Jennings* [1987] reported a change in the abundance of vents following a 7 magnitude earthquake in northern California. In the Gulf of Izmit, similar observations were made related to the 7.4 magnitude, 17 August 1999 earthquake [*Alpar*, 1999; *Cormier et al.*, 2006], based on high-resolution seismic profiles and water column imagery, with an increase of the released methane intensity [*Kusçu et al.*, 2005]. In the Gulf of Patras, higher methane concentrations were measured following an earthquake in 2003 in the surroundings of a known active giant pockmark [*Christodoulou et al.*, 2003; *Hasiotis et al.*, 1996; *Soter*, 1999]. It is the change in gas levels, rather than the presence of gas, that indicates a causative relationship to the earthquake [*Field and Jennings*, 1987]. In the Gulf of Izmit, away from the failure sites, gas was indeed present in the sediment and in the water column prior to and after the earthquake [*Kusçu et al.*, 2005]. In some places, a decrease in gas seeping over time was observed, most likely related to fluid migration. More recently, nonseismic signals recorded by ocean bottom seismometers within 10–30 Hz have been proposed to be related to gas escape through the seabed in the Sea of Marmara [*Bayrakci et al.*, 2014; *Tary et al.*, 2012]. These observations raise the following basic question: How does the expulsion of fluids and their fluxes evolve through time and space prior to and after a seismic event?

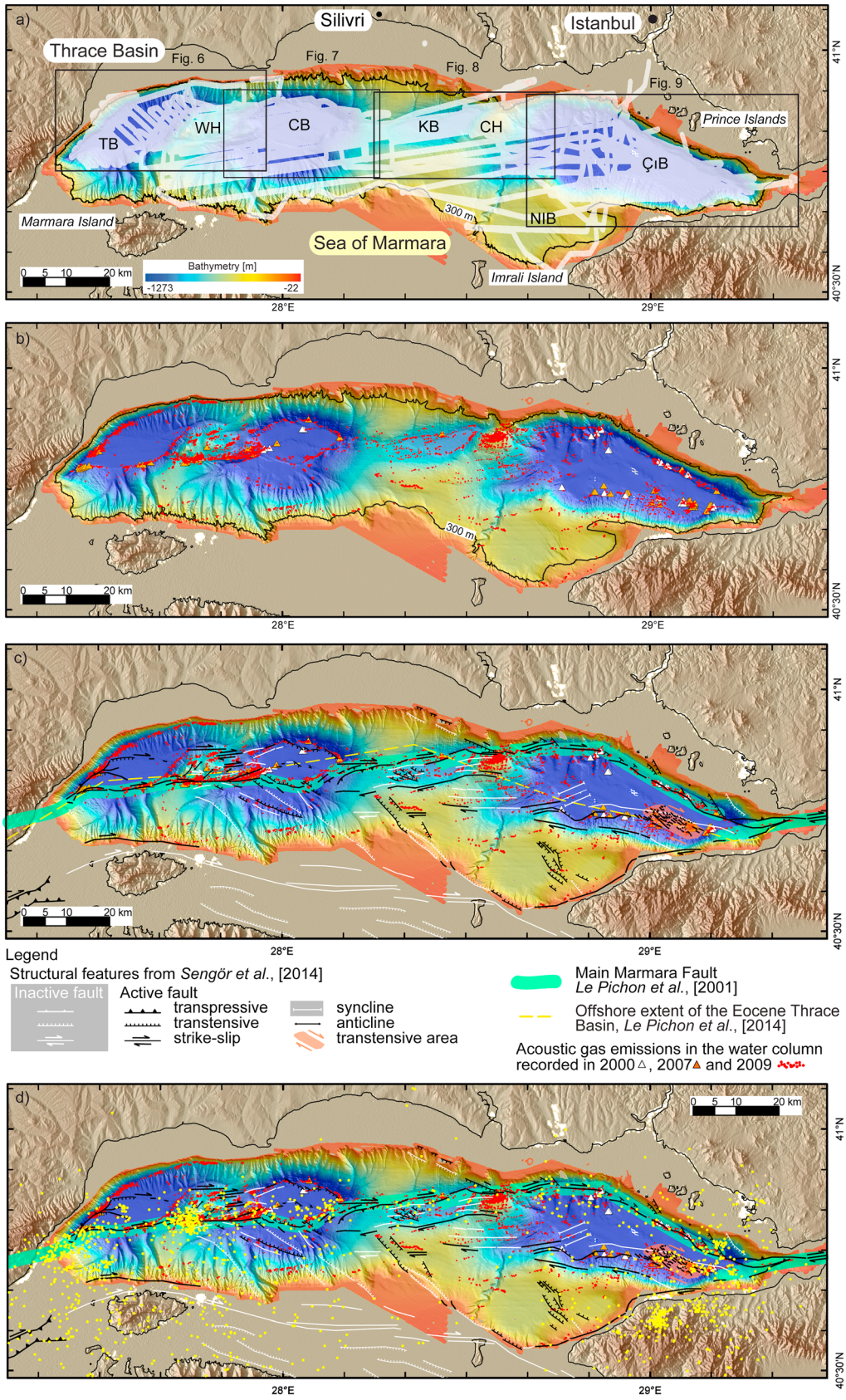
a)
Silivri
Istanbul
Thrace Basin
Fig. 6
Fig. 7
Fig. 8
Fig. 9
TB
WH
CB
KB
CH
ÇıB
NIB
Prince Islands
Marmara Island
Sea of Marmara
Imrali Island
300 m
Bathymetry [m]
-1273
-22
0 5 10 20 km
28°E
29°E
41°N
40°30'N
b)
c)
Legend
Structural features from Sengör et al., [2014]
Inactive fault
Active fault
transpressive
transtensive
strike-slip
syncline
anticline
transtensive area
Main Marmara Fault
Le Pichon et al., [2001]
Offshore extent of the Eocene Thrace Basin, Le Pichon et al., [2014]
Acoustic gas emissions in the water column recorded in 2000 △, 2007 ▲ and 2009
d)

Figure 4

The presence of gas escapes through the deep Marmara seafloor was first inferred from acoustic data collected using a side-scan sonar during the Marmara 2000 expedition of R/V *Le Suroît* [*Géli et al*., 2008] (Figure 2) and from near-seafloor visual observations made with the Victor 6000 remotely operated vehicle during the Marmarascarps 2002 expedition [*Armijo et al*., 2002; *Zitter et al*., 2008]. A further acoustic investigation with the use of a Simrad EK60 echo sounder was performed in 2007 during the Marnaut expedition (Figure 2). A near-bottom seafloor investigation with the *Nautile* submersible was also conducted during the same cruise (Figure 3) [see, e.g., *Grall*, 2013; *Tryon et al*., 2012]. In situ gas sampling (Figure 3a) was performed in different places of the Sea of Marmara, including the Çınarcık Basin, Central High and the Western High, where gas hydrates were recovered at a water depth of 666 m [*Bourry et al*., 2009]. Isotopic analysis revealed a predominant thermogenic origin for the collected fluids on the two highs and for the gas hydrates [*Bourry et al*., 2009; *Ruffine et al*., 2012], with both sites having a contribution of biogenic methane resulting from biodegradation of oil and methanogenesis at the reservoir level (L. Ruffine, personal communication, 2014). Mainly biogenic methane mixed with a small amount of thermogenic ethane characterizes the Çınarcık Basin site [*Bourry et al*., 2009] (Figure 2). Many cold seeps in the Sea of Marmara are associated with authigenic carbonates [*Crémière et al*., 2012], mainly in relation to the anaerobic oxidation of methane (AOM) [*Chevalier et al*., 2011]. However, analyses of gas samples from the Central High and the southern Çınarcık Basin suggest the occurrence of anaerobic oxidation of nonmethane hydrocarbons, including oil [*Chevalier et al*., 2011]. The spatial distribution of fluids inferred from the 2000 and 2007 acoustic data sets that were focused on restricted insonified areas [*Géli et al*., 2008] has been significantly updated using the large 3-D water column imagery data set acquired in late 2009 with the hull-mounted multibeam echo sounder onboard the R/V *Le Suroît* (Figure 2 versus Figure 4).

3. Systematic, 3-D Acoustic Imaging of the Water Column

3.1. Water Column Multibeam Acquisition

Shipborne multibeam surveys of the water column in the Sea of Marmara were conducted to systematically map the distribution of seafloor gas emissions at the scale of the sea (Figure 4a). This was performed onboard the R/V *Le Suroît* during the Marmesonet expedition (2009) as part of the ESONET (European Seas Observatory NETwork) Marmara demonstration mission (Marmara-DM) project. The seafloor and water column data were acquired with a Kongsberg EM302 multibeam echo sounder (27–33 kHz, 288 beams, emission and reception angles of 1° and 2°, 2 or 5 ms pulse length), with automatic swath width control and an equidistant sounding pattern over water depths varying from 300 to 1270 m. Volume backscattering coefficients related to the water column records were stored along more than 4500 km of acoustic tracks. This type of acquisition, unlike single-beam echo sounders [*Dupré et al*., 2014a] and side-scan sonars [*Dupré et al*., 2010; *Géli et al*., 2008], are very efficient for the coverage of wide areas (Figure 4b versus Figure 2). Data were collected during two legs from the 4 November 2009 to the 14 December 2009, with 21 full days of acquisition, covering ~2900 km^2 equivalent to 70% of the deepest parts of the Sea of Marmara, where water depths exceed 300 m (Figure 4a).

3.2. Water Column Multibeam Data Processing and Identification of Gas Flares

The 3-D acoustic acquisition of the water column using multibeam systems was at its beginning in 2009. Significant efforts were made to develop tools for the postacquisition work flow, including the display (e.g., polar echograms, Figure 5), replay, processing, and analysis of the Marmesonet data set, leading to the development of a software platform combining Sonarscope, a Matlab-based program and a 3-D Viewer called Sonarscope3DViewer [*Augustin*, 2011] (Figure 5). Algorithms were developed to replay and process the echograms by improving the signal-to-noise ratio (Figure 5a versus Figure 5b) in order to pick up

Figure 4. (a) EM302 water column multibeam track lines during the 2009 Marmesonet expedition. The white buffer along the navigation stands for the insonified zone within which gas bubbles are detectable. TB, Tekirdağ Basin; WH, Western High; CB, Central Basin; CH, Central; KB, Kumburgaz Basin; ÇıB, Çınarcık Basin; NIB, North Imrali Basin. (b) The 2-D Marmara shaded bathymetry map with gas flare distribution, (c) fault networks from *Şengör et al*. [2014] with the offshore extent of the Eocene Thrace Basin from *Le Pichon et al*. [2014], and (d) microearthquake epicenters (yellow dots) recorded between 2005 and 2011 [*Şengör et al*., 2014; H. Karabulut, personal communication, 2014]. White, orange, and red marks stand for water column acoustic anomalies recorded in 2000, 2007, and 2009, respectively. The maps illustrate the 2009 seepage activity over more than 1 month (from 4 November 2009 to 14 December 2009). Each of these acoustic anomalies is displayed as a 150 m radius red dot.

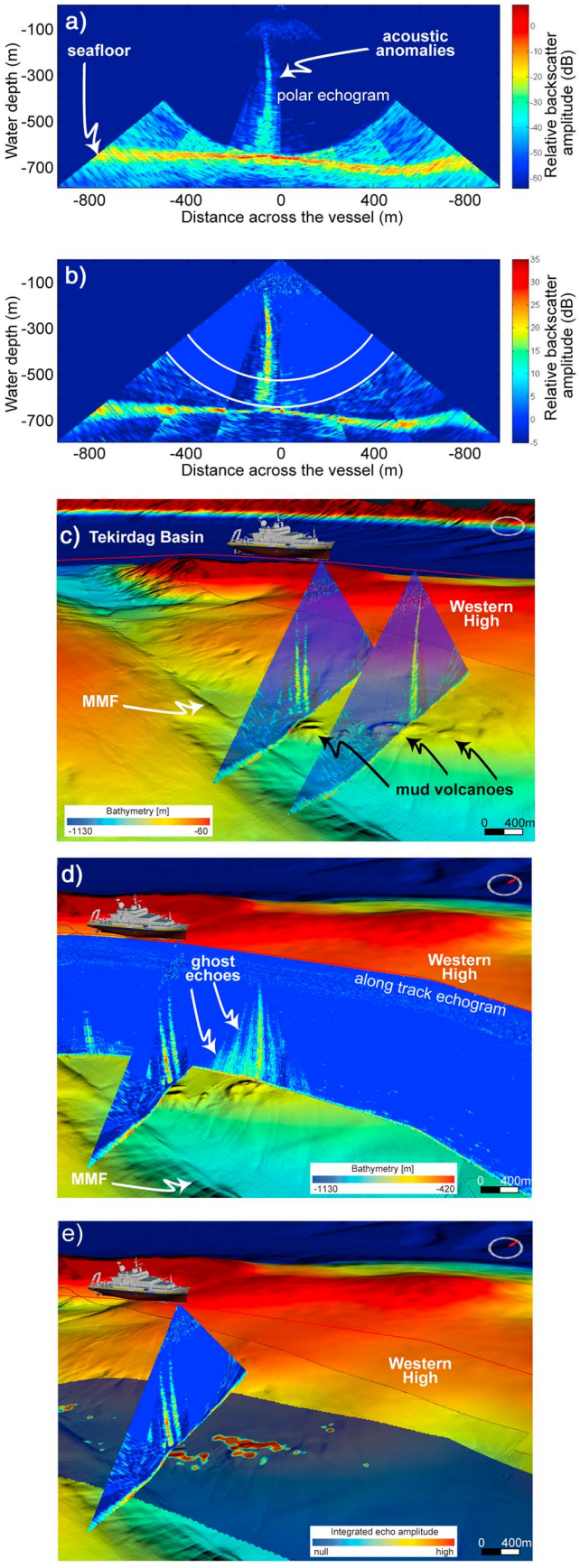

events in the water column (e.g., root flares on the seabed) and accurately localize these events (e.g., Figures 5c and 5d). Moreover, processing of the acoustic water column data included echo integration of the signal, similar to the methods used in fishery acoustics [*Dragesund and Olsen*, 1965]. The echo intensity was integrated over a selected slice within the water column (see the white slice in the polar echogram in Figure 5b) and was projected on the seafloor's surface to get a 2-D cartographic representation of the data (Figure 5e). This new 2-D display of the water column data is of great help in imaging and understanding the complex structure of gas emission fields (Figures 5c and 10). In particular, such a representation helps to distinguish real echoes from ghost echoes (Figure 5d).

The EM302 multibeam echo sounder was able to accurately detect water column echoes within the entire water

Figure 5. (a) Raw and (b) processed polar echograms from EM302 multibeam echo sounder water column data (Sonarscope © Ifremer). The acoustic anomalies recorded in the water column are echoes caused by escaping gas bubbles through the seafloor. They are located at water depth of 660 m in the Western High above an active mud volcano complex close to the North Anatolian fault (~between 250 and 650 m) (Figure 5c). The acoustic imprint of the highest plume almost reaches the surface with a height of 600 m above the seabed. The 3-D views of the seabed and water column (Sonarscope 3DViewer © Ifremer) with (c) geo-referenced processed polar echograms (left-hand side one is displayed in Figure 5b), (d) an along-track water column echogram, and, with the same perspective, (e) a mosaic of echo integration with water column echo intensity integrated over a 135 m thick vertical slice (white in Figure 5b), and this, 5 m above the seafloor to avoid echoes and artifacts in relation to the seabed. Note that the R/V *L'Atalante* (courtesy of Altran) is not drawn to scale. The background bathymetry was acquired in 2000 (Marmara expedition) with a Kongsberg EM300 multibeam echo sounder, while the high-resolution bathymetry was recorded in 2009 (Marmesonet expedition) with an EM2000 echo sounder mounted on the AsterX AUV (Ifremer). The red line stands for the ship navigation and the North corresponds to the red arrow in the white circle (Figures 5c–5e).

depth range of the Sea of Marmara with tens of thousands of gas bubble streams identified (Figure 4b). The detection was optimized for the central beams, but flares with strong backscatter intensity and a large imprint could also be imaged with the outer beams. The acoustic anomalies were caused by the presence of gas bubbles within the water column due to the impedance contrast between the gas bubbles and the surrounding water [*Dupré et al*., 2010; *Merewether et al*., 1985; *Paull et al*., 1995]. The foot of each gas flare detected in the water column was precisely localized in latitude and longitude and was marked as a 150, 100, or 50 m radius circle depending on the scale of the map (Figures 4b, 6a, 7, 8a, and 9). The associated footprint is therefore suitable for proper display and, moreover, takes into account any uncertainty in the localization induced by the event picking. Many of the numerous and widespread gas flares that were recorded at the scale of the Sea of Marmara reach several hundreds of meters above the seafloor, attesting to a vigorous seepage activity with high fluid fluxes (e.g., Figure 5) and questioning about the fate of the gas in the water column and potentially in the atmosphere, a topic not addressed in this paper.

4. Spatial Distribution of Gas Emissions at the Scale of the Sea of Marmara

Different fault maps, based on seismic data and on structural interpretation, have been published since the late 1990s [e.g., *Carton et al*., 2007; *Görür and Elbek*, 2013; *Grall et al*., 2012; *İmren et al*., 2001; *Laigle et al*., 2008; *Le Pichon et al*., 2014; *Le Pichon et al*., 2001; *Okay et al*., 1999; *Parke et al*., 2002; *Şengör et al*., 2005, 2014]. In this paper, we use the maps that *Grall et al*. [2012] (Figure 1b) and *Şengör et al*. [2014] (Figure 4c) recently published. Both papers present a synthesis of the fault networks at the scale of the Sea of Marmara but at different resolutions. The superposition of gas seeps on top of the fault map from *Şengör et al*. [2014] (Figures 4c, 6a, 7, 8a, and 9) provides a general picture of the gas distribution in relation to the faults, active or inactive, as well as to other geological features.

4.1. Main Marmara Fault

Along the Main Marmara Fault [*Le Pichon et al*., 2001; *Şengör et al*., 2014], gas flares were detected from the Gulf of Izmit in the east to the western edge of the Tekirdağ Basin, where the NAF enters the Isthmus of Gallipoli (Figure 4). The seepage activity, however, does not appear homogeneous, as the density of gas flares varied along the fault trace. Gas emissions can be particularly numerous within some segments of the fault valley, for instance, as the strike-slip segment cuts across the Western High (Figure 6), with continuous emissions along the fault trace. Some other segments of the NAF were loci of relatively moderate seepage activity (e.g., Kumburgaz segment, Figure 8), while some relatively short ($<$5 km) segments were not characterized at all by fluid escape. This was the case for the segment connecting the Central High to the Kumburgaz Basin (Figure 8), as well as for other segments in the northwestern border of the Çınarcık Basin (Figure 9) and along the Tekirdağ Basin edges (Figure 6).

The widespread distribution of gas emissions in the Sea of Marmara is detailed hereafter, sector by sector, from west to east (Figure 4a).

4.2. Tekirdağ Basin and Western High

Numerous acoustic anomalies have been observed along the edges of the Tekirdağ Basin (Figure 6a). Dense and closely spaced gas emissions characterized parts of the base of the western and northern escarpments and along the eastern edge of the Tekirdağ Basin bordering the Western High. Gas emissions appeared to be unevenly distributed along the strike-slip segment of the Main Marmara Fault to the south of the basin and along the northern flank, with sparse acoustic anomalies within canyons on both of these flanks. In contrast, only two isolated gas emission sites have been detected within the inner part of the Tekirdağ Basin.

The Western High is delimited by the main trace of the current Main Marmara Fault (MMF) in the south and E-W running faults in the north (Figure 6). The southern branch of the Main Marmara Fault valley, all the way across the Western High, from the Tekirdağ Basin to the Central Basin borders, is mostly characterized by closely spaced, vigorous gas emission sites (Figures 6 and 7), with several swarms of highly active and dense gas emissions (Figures 5 and 6). The northern E-W branch of the MMF, with its relatively minor tectonic activity, did not have as many gas seeping sites compared to the southern segment. No gas emissions were recorded in the eastern side of the northern branch (Figure 6a). However, numerous gas emissions were found on the Western High in the area between these two fault branches in association to a variety of topographic structures, described hereafter.

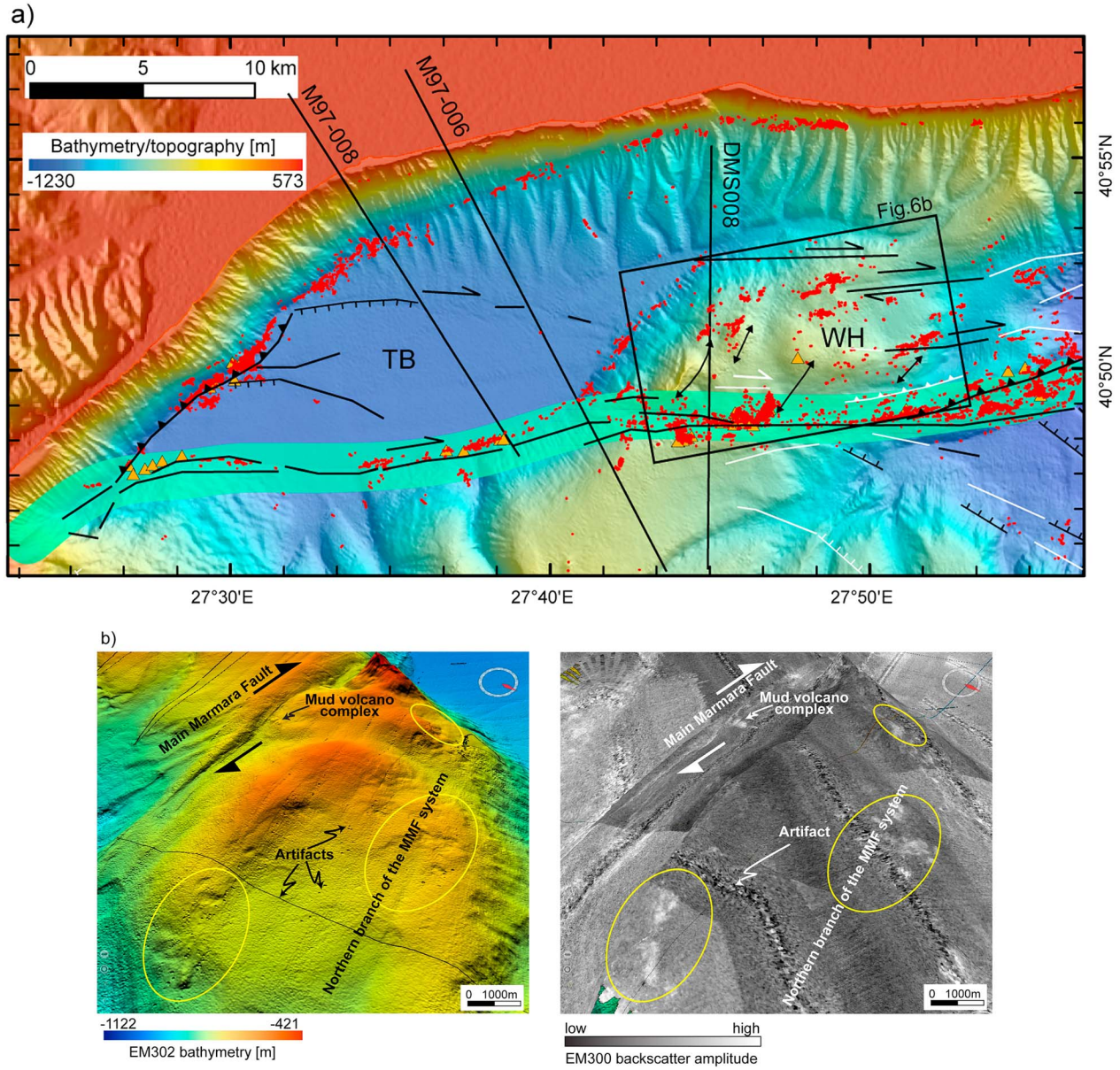

Figure 6. (a) Water column acoustic gas anomaly distribution in the Tekirdağ Basin and Western High. White, orange, and red marks stand for water column acoustic anomalies recorded in 2000, 2007, and 2009, respectively. The EM302 multibeam acoustic anomalies were recorded between 4 November 2009 and 14 December 2009. Each of them is displayed as a 50 m radius circle. Multichannel seismic profiles discussed in the text are reported (M97-006 and DMS008 [*İmren et al.*, 2001] and M97-008 [*Parke et al.*, 2002]). See Figure 4 for complete legend. (b) The 3-D shaded bathymetric view of the Western High (EM302 multibeam data, Marmesonet 2009) (top) draped with backscatter data (EM300 multibeam data, Marmara 2000 [*Rangin et al.*, 2001]) (bottom) with a vertical exaggeration of 4 (Sonarscope/3DViewer © Ifremer). Yellow circles stand for areas characterized by seafloor depressions, a destabilized upper sediment cover, high-backscatter seabed amplitudes, and water column acoustic gas emissions (Figure 6a).

On the southern side of the current MMF, active sites were mainly found either in relation to slope instabilities, or along the axis of a fold parallel to the MMF, within less than 1 km from the present-day seabed fault trace. On the northern side of the current MMF, up to 8 km away from the fault trace, acoustic gas anomalies were distributed all over the Western High on small-scale reliefs orientated SSW-NNE and WSW-ENE along the trend of folds and thrusts, deforming the Western High [*İmren et al.*, 2001] or subparallel to the MMF. One of the seep-related swarms connected to the MMF corresponds to a mud volcano complex located north of the MMF (Figure 6) [*Grall et al.*, 2013; *Thomas et al.*, 2012]. This mud volcano complex composed of three main structures exhibited a relatively high level of activity in terms of

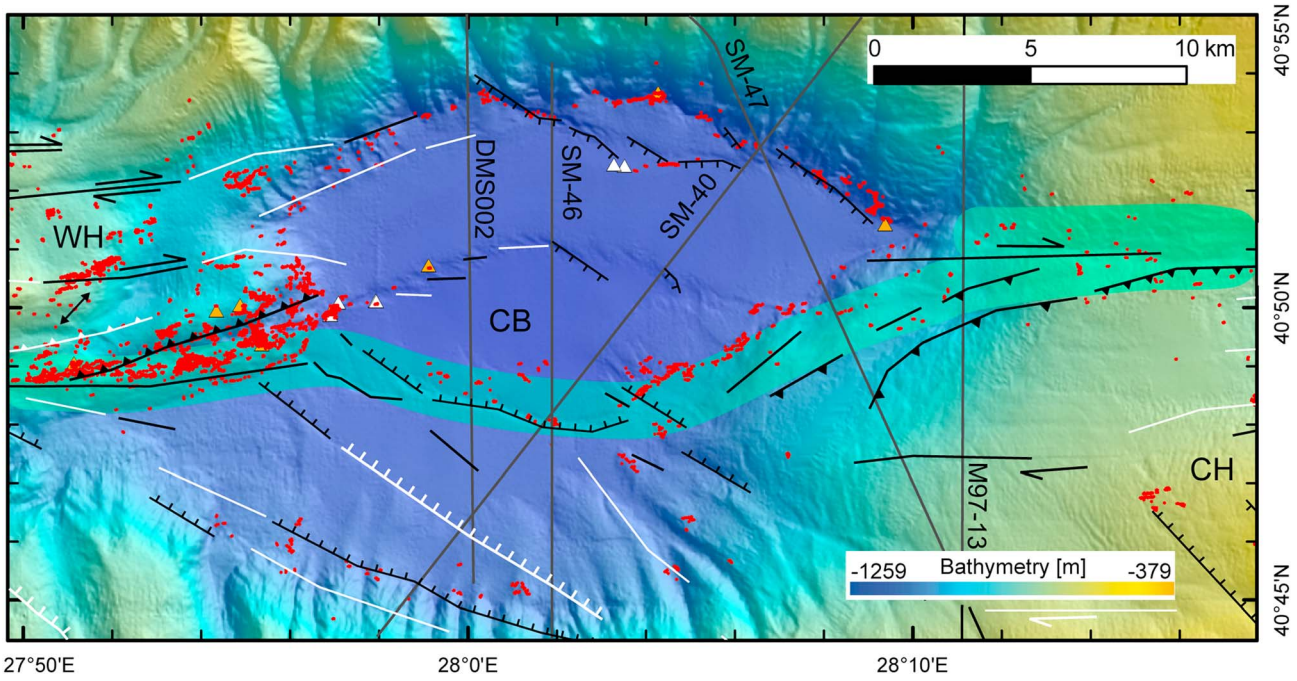

Figure 7. Water column acoustic gas anomaly distribution in the Central Basin. White, orange, and red marks stand for water column acoustic anomalies recorded in 2000, 2007, and 2009, respectively. The EM302 multibeam acoustic anomalies were recorded between 4 November 2009 and 14 December 2009. Each of them is displayed as a 50 m radius circle. Multichannel seismic profiles discussed in the text are reported (SM-46 and 47 [*Bécel et al*., 2010], DMS002 and M97-13 [*İmren et al*., 2001; *Parke et al*., 2002], and SM-40 [*Laigle et al*., 2008]). See Figure 4 for complete legend.

gas expulsion, with gas escapes occurring at the surface of three main mud volcanoes, as well as in their close surroundings (Figures 5 and 6). Acoustic gas emissions were also, in some places, correlated with small-scale traces of landslides and, in particular, in the zone located between the southern and northern branches of the MMF. There, a few swarms of gas emissions were present that were associated with seafloor depressions, destabilized upper sediments and areas of high-backscatter seafloor amplitudes (see yellow circles in Figure 6b).

4.3. Central Basin

The Central Basin is a composite basin [*Grall et al*., 2012] formed from NW-SE trending en échelon normal faults connected by now-largely abandoned E-W strike-slip segments, possibly R shears that were part of the older North Anatolian Shear Zone [*Rangin et al*., 2004; *Şengör et al*., 2005, 2014]. Within it, there is a spindle-shaped negative flower structure outlining a smaller basin, hereafter the inner basin (Figures 4c and 7).

The maximum density of acoustic anomalies was found in the western side of the basin along the Main Marmara Fault's 9 km long segment connecting the Western High to the Central Basin (Figure 7). Within the basin itself, acoustic anomalies were unevenly distributed, the greatest density being found on the northern edges of the outer structure and along the southern edges of the inner, spindle-shaped basin. In some cases, acoustic anomalies appeared to be located within submarine valleys.

On the edges of the Central Basin, gas emissions were generally found at the base of the 1 km high escarpments. The pattern of gas emissions apparently depends on the characteristics of the bordering fault segments. Along the NE-SW striking fault segments that border the northwestern side of the outer basin, gas emissions were ubiquitously distributed. Gas emissions are frequent along the eastern edge of the Central Basin toward the Central High, where several strike-slip fault branches form a positive flower structure (see seismic profiles SM-47 [*Bécel et al*., 2010] and M97-13 [*İmren et al*., 2001; *Parke et al*., 2002]) (Figure 7). It is yet unclear whether a fault is present all along the NE-SW striking slope break [*Şengör et al*., 2014] where gas emissions were observed. Along the SE-NW escarpment that borders the northeastern

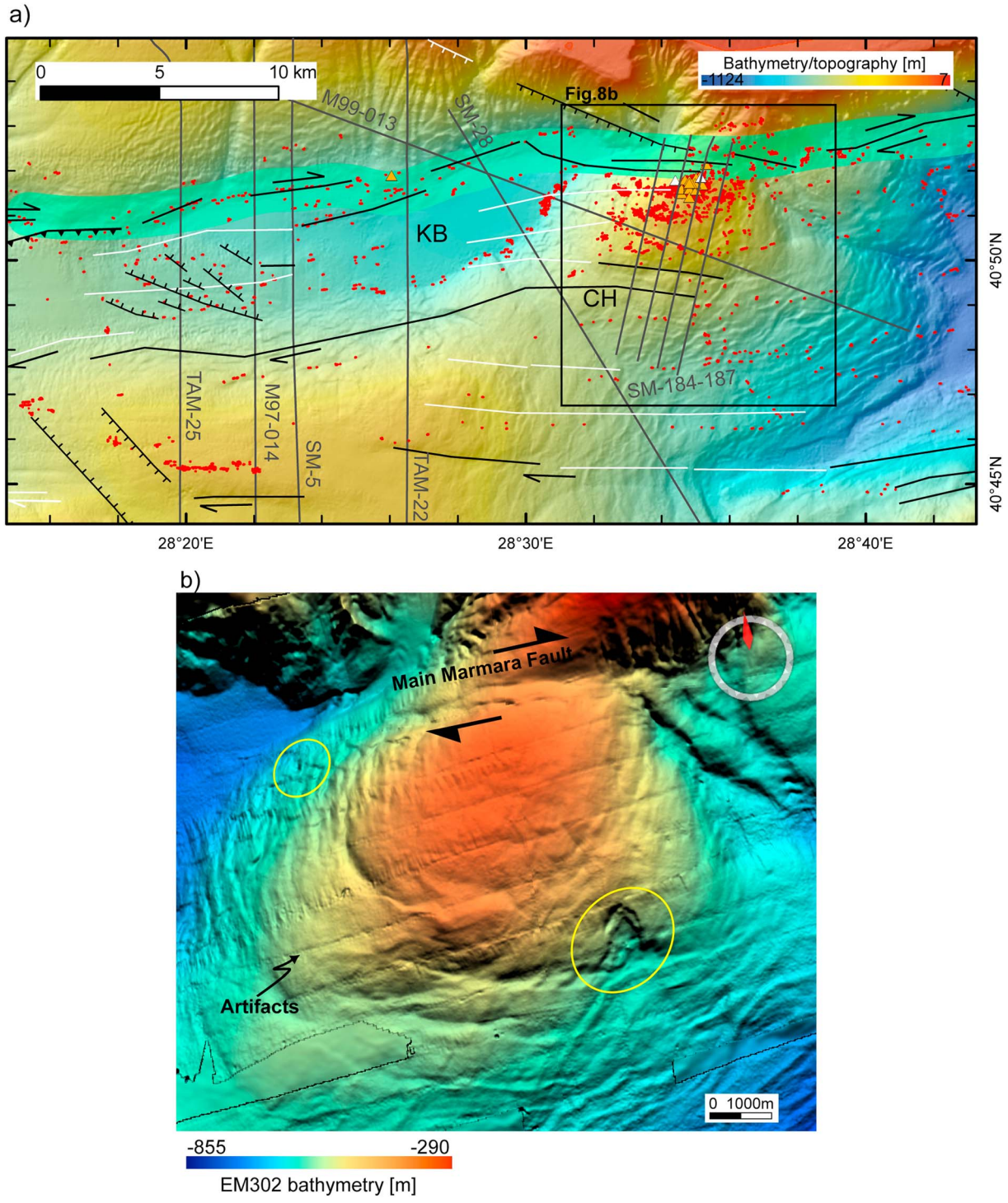

Figure 8. (a) Water column acoustic gas anomaly distribution in the Kumburgaz Basin and Central High. White, orange, and red marks stand for water column acoustic anomalies recorded in 2000, 2007, and 2009, respectively. The EM302 multibeam acoustic anomalies were recorded between 4 November 2009 and 14 December 2009. Each of them is displayed as a 50 m radius circle. Multichannel seismic profiles discussed in the text are reported (SM-5 and 28 [*Bécel et al.*, 2010], M97-014 and M99-013, SM-184 to 187 [*Carton et al.*, 2007; *İmren et al.*, 2001], TAM-22 [*Shillington et al.*, 2012], and TAM-25 [*Sorlien et al.*, 2012]). See Figure 4 for complete legend. (b) The 2-D shaded bathymetric view of the Central High (EM302 multibeam data, Marmesonet 2009) with a vertical exaggeration of 4 (Sonarscope/3DViewer © Ifremer). Yellow circles stand for some areas characterized by a destabilized upper sediment cover and landslide scars. The southern slide does not reveal any water column and seabed backscatter anomalies, whereas the northern slide is characterized by an acoustic gas flare and high-backscatter seafloor.

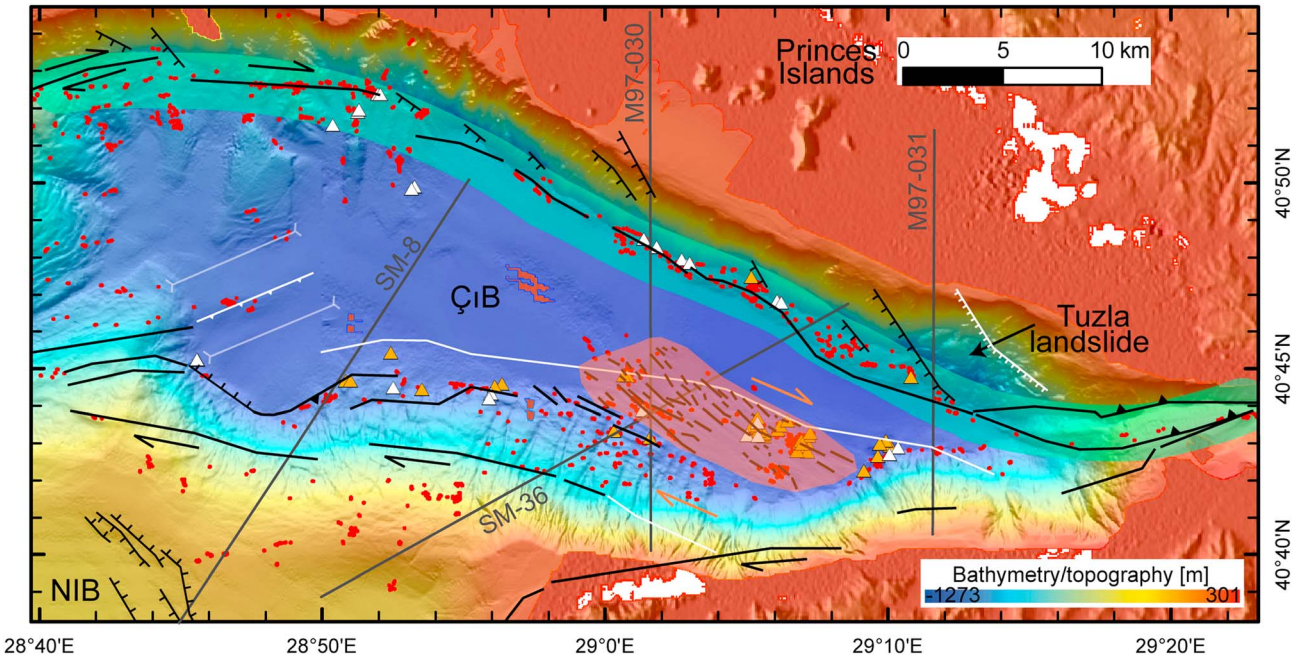

Figure 9. Water column acoustic gas anomaly distribution in the Çınarcık Basin. White, orange, and red marks stand for water column acoustic anomalies recorded in 2000, 2007, and 2009, respectively. The EM302 multibeam acoustic anomalies were recorded between 4 November 2009 and 14 December 2009. Each of them is displayed as a 100 m radius circle. Multichannel seismic profiles discussed in the text are reported (M97-31 [*İmren et al.*, 2001], M97-30, SM-8 and 36 [*Laigle et al.*, 2008; *Parke et al.*, 2002]). See Figure 4 for complete legend.

side of the outer basin, gas emissions were found on the strike-slip fault segments connecting the en échelon system of normal faults. Along the SE-NW striking southern edge, gas emissions were relatively sparsely distributed.

On the northern edges of the inner basin, gas emissions were found only near the western and eastern extremities, where the MMF segments connect to the Central Basin. In contrast, on the southern edges, gas emissions were (i) densely distributed along the NE-SW-oriented, side-stepped, strike-slip fault segment bordering the inner structure to the southeast and (ii) scarcely distributed along the NW-SE-oriented normal fault segments bordering the structure to the southwest (see seismic lines SM-46 [*Bécel et al.*, 2010; *Grall et al.*, 2012] and SM-40 [*Laigle et al.*, 2008]). Gas emissions were also found on some striking NNW-SSE en échelon normal faults affecting the sedimentary cover.

4.4. Kumburgaz Basin and Central High

The Central High is a "comma-shaped," topographic structure separating the Central Basin from the Çınarcık Basin (Figures 2 and 8a). The western part of the Central High is an east-west trending structure between the Central Basin and longitude 28°31′N. East of this longitude, the eastern termination of the Central High consists of a dome-shaped anticline centered near 40°51.3′N–28°35′E (also called the "Central Marmara Ridge" by some authors [e.g., *Sorlien et al.*, 2012]), that is crosscut by the Main Marmara Fault (Figure 8b). The Kumburgaz Basin is an elongated, SSW-NNE-orientated, perched syncline, bordered by the Central High to the south and east, and by en echelon segments of the Main Marmara Fault to the north (e.g., seismic lines M97-14 [*İmren et al.*, 2001; *Rangin et al.*, 2004], TAM-22 [*Shillington et al.*, 2012], and TAM-25 [*Sorlien et al.*, 2012]) (Figure 8a). The MMF defines a negative flower structure at some places as it reaches the surface (seismic line SM-28 [*Bécel et al.*, 2010]) (Figure 8a). Between the Kumburgaz Basin and the Central Basin (to the west), the MMF splits into at least three branches, forming a positive flower structure (e.g., seismic line SM-47 [*Bécel et al.*, 2010; *Rangin et al.*, 2004]), above which gas emissions occurred (Figure 7).

Gas emissions were found along the borders of the Kumburgaz Basin but with a relatively moderate activity (Figure 8a). Along the northern border, gas emissions occurred along only part of the surface trace of the Main Marmara Fault. The active strike-slip fault segment bordering the basin to the south was

unfortunately not insonified (Figure 4a). Most of the seeps appear then located at the base of the escarpment around the basin, from the northeastern to the western side without ruling out possible gas emissions along the southern fault. East-west trending lineaments of gas emissions were also present on the western part of the Central High (west of 28°35′E), with no visible fault control in depth (Figure 8a) (seismic line SM-5 in *Bécel et al.* [2010] and *Şengör et al.* [2014]). Along the 9 km of the MMF segment connecting the Kumburgaz Basin to the Central High, gas escapes were relatively rare and were even absent along the 3 km long segment located in the western Central High (west of 28°34.8′E). The highest density of gas emissions was present on top of the circular-shaped, anticline structure [*İmren et al.*, 2001], centered near 40°51.3′N–28°35′E. Gas escapes occurred away from the trace of the MMF farther north and mainly southward. The highest density of gas emissions was recorded 3 km away, south of the MMF fault trace (Figure 8a). The bathymetry also revealed (i) a folded seabed, implying a disturbed upper sedimentary cover and (ii) in some places, landslides along the slope of the anticline (Figure 8b).

4.5. Çınarcık Basin and North İmralı Basin

On the NW side of the Çınarcık Basin, gas emissions defined an E-W trending lineament connecting the northern Çınarcık escarpment to the Central High (Figure 9). This lineament follows the trace of the Main Marmara Fault to the west of the bend located near 28°53′E. On the northeastern edge of the Çınarcık Basin, gas emissions preferentially occurred along a topographic bench (all earthquake first-motion solutions here indicate strike slip [*Bohnhoff et al.*, 2013; *Bulut et al.*, 2009; *Karabulut et al.*, 2011]), covered by recent sediments, located between the base of the cliff, where the Paleozoic basement outcrops and the main active fault scar [*Grall*, 2013]. As the width of the bench decreases toward the NW direction (from 1.8 to 0 km), gas emissions become less dense. To the NW of 40°50.3′N–28°56.8′E, along a 5 km long segment that exhibits no bench, no gas emissions were documented. Gas emissions were found at the toe (and only there) of the mass-wasting features that *Zitter et al.* [2012] identified along the southern border of the Çınarcık Basin, as well as at the toe of the Tuzla landslide (Figure 9). On the southern edge, seeps mainly associated with biogenic methane emissions [*Bourry et al.*, 2009] occurred on en échelon normal faults that trend ~N130°–N140° and were distributed in a 2–4 km wide swath oriented N100°. This corresponds to an "inner boundary fault" [*Carton et al.*, 2007; *Le Pichon et al.*, 2001] located in the westward continuation of the Izmit segment (Figure 9).

Although the southern part of the Sea of Marmara was not systematically covered, the data revealed numerous sites where gas escaped from the seabed. This was unknown from previous surveys (Figure 2) [*Géli et al.*, 2008]. Gas emissions appeared in some parts of the North Imralı Basin area, e.g., along the southern border, in relation to canyons (see, e.g., north of the İmralı Island in Figure 4) and over the topographic high between the North Imrali Basin and the Çınarcık Basin (Figures 4 and 9). Unfortunately, the data coverage in this area is still insufficient (Figure 4b). The effect of bias related to profile implementation in the North Imrali Basin area does not allow any interpretation with regard to fault control as the detected seeps are obviously aligned along the ship track unlike the other investigated areas that are densely covered.

4.6. Spatiotemporal Variations of Fluid Emissions

The different acoustic surveys collected in 2000, 2007, and 2009, despite the differences in data coverage and in acquisition systems, provide insights into the temporal variability of the seepage activity (Figures 4 and 6–9). The comparison between the available time windows (2000, 2007, and 2009) indicates an overall persistence of the seepage activity within the entire Sea of Marmara. During the 2009 Marmesonet expedition (4 November 2009 to 14 December 2009), some areas were surveyed several times, revealing variations in the spatial distribution and intensity of the seepage activity on the scale of a few hours to a few days (Figure 10). Between 2007 and 2009, a spatial shift of the seepage activity seems to have occurred along part of the segment of the current MMF bordering the southern edge of the Tekirdağ Basin, where an eastward shift of 3 km is observed along the fault trace (Figure 6). Locally, spatial shifts of seeps may have occurred, as indicated by the distribution of gas emission sites in 2000, 2007, and 2009, in the eastern side of the southern border of the Çınarcık Basin. These are, however, associated with smaller distances of ~500 m (Figure 9). Based on the limited comparative data set available, it appears, however, that the only temporal variations observed, not related to the positioning systems, are located at both sides of the Sea of Marmara, in the Tekirdağ and Çınarcık basins.

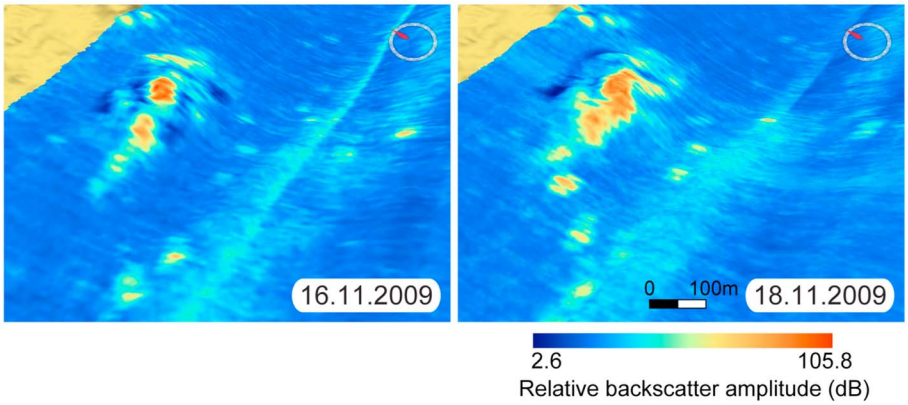

Figure 10. Temporal variability of the seepage activity at a daily time scale, as illustrated by two shipborne multibeam echo sounder paths from a 2 day interval above an active mud volcano complex located in the Western High (Figures 5 and 6). The 3-D view maps are 2 m pixel grid mosaics of the echo-integrated water column draped on the EM302 multibeam bathymetry with a vertical exaggeration of 3 (water depths range from 664 to 737 m). The signal has been echo integrated on processed and compensated polar echograms along a 100 m thick water column slice at 5 m above the seafloor. See details of the echo integration principle in the text therein. Both maps are derived from the same multibeam acquisition configuration and exhibit differences in water column backscatter amplitudes, enlightening the variability in space of the gas emissions and of the related fluxes.

5. Discussion

5.1. Multiparameter Signature of Fluid Systems

A correlation exists between the presence of gas bubbles in the water column detected on the acoustic records (Figure 4c) and (i) the occurrence of seep-related structures from visual observations [e.g., *Armijo et al.*, 2005; *Zitter et al.*, 2008] (Figure 3) and sonar seabed imagery [e.g., *Géli et al.*, 2008; *Rangin et al.*, 2001] (Figure 6b); (ii) the presence of discontinuities in the sediment cover (e.g., landslides) [*Zitter et al.*, 2012] (Figures 6b, 8b, and 9); (iii) the evidence of gas-saturated sediments identified on high-resolution (chirp) seismic data [e.g., *Tary et al.*, 2012]; and (iv) the fault network imaged at depth by seismic profiles [e.g., *Bécel et al.*, 2010; *Carton et al.*, 2007; *İmren et al.*, 2001; *Laigle et al.*, 2008; *Le Pichon et al.*, 2001; *Parke et al.*, 2002; *Şengör et al.*, 2014; *Shillington et al.*, 2012; *Sorlien et al.*, 2012].

Numerous gas emission sites were discovered in 2009 only based on acoustic records of the water column with the shipborne multibeam echo sounder (Figure 4c versus Figure 2). On the Western High, for instance, a few swarms of gas emissions associated with seafloor depressions destabilized upper sediments in the Chirp profiles, and areas of high-backscatter amplitudes, based on shipborne multibeam data sets (see yellow circles in Figure 6b), were definitively active-seeping sites that were most likely associated with gas-saturated sediments and precipitation of methane-derived carbonates. Two processes are possible there and may occur concurrently: sediment scars may open pathways for gas migration up to the surface, and the upward migration of gas may induce slope instabilities. Active seeps are generally characterized by high-backscatter amplitude of the seabed (due, e.g., to authigenic precipitates, disturbed microrelief at the seabed, and gas-saturated sediments; [*Dupré et al.*, 2010; *Foucher et al.*, 2010]), but this is not always the case [*Dumke et al.*, 2014]. Indeed, the backscatter signature mainly depends on the sonar parameters (frequency and resolution). The gas escaping areas in the Central High are characterized by relatively low seafloor backscatter amplitudes, similarly to the inactive surrounding seabed areas. This may be explained by low contents of gas and carbonate concentrations within the uppermost sediments (a 30 kHz signal penetrates up to a few meters) and may indicate recently born seeps. The water column backscatter from shipborne multibeam is the most efficient tool for detecting seeping sites by 3-D imaging the water column in a short period of time and providing evidence for the seepage activity, even in recently formed areas.

The numerous multichannel seismic reflection profiles across the Sea of Marmara revealed the presence of faults below the seabed (e.g., synthesis fault map by *Şengör et al.* [2014]), where gas bubbles were acoustically recorded in the water column (Figure 4), as previously exposed. In some cases, the seismic

signal is very much disturbed by the presence of gas within the sediments, which does not permit proper imaging of the fault (e.g., line M97-030 across the northeastern edge of the Çınarcık Basin, Figure 9, [*Parke et al*., 2002]). Faults previously seen as buried without reaching the seabed may be reinterpreted on the basis of gas escape occurrence above (e.g., line M99-013 across the Central High, Figure 8, [*İmren et al*., 2001]). In these latter cases, the main fault at depth may lead to fracturing and dispersion of the gas in the uppermost sediments due to changes in the mechanical properties of the sediments. The distribution of gas escapes through the seabed could help to better define the trace of faults, active or inactive, and may be a substantial guide in areas with sparse seismic lines or in the case of disturbed environment (e.g., with seismic gas wipeouts).

5.2. Factors Controlling the Distribution of Gas Emissions

Gas emissions are controlled by the following combined factors: the tectonic regime, the sedimentary cover, and the connections with the gas source.

5.2.1. Tectonic Control

Gas seeps in the Sea of Marmara are widespread (Figure 4) and are commonly observed along (i) known fault scarps, (ii) the major portion of the MMF, (iii) the edges of the four deep basins (Tekirdağ, Central, Kumburgaz, and Çınarcık basins, Figures 4–9) whether or not they are in relation to the main current fault trace of the MMF, and (iv) in relation to topographic highs, more precisely, in relation to anticlines acting as gas traps (see, e.g., on the Western and Central highs, Figures 6a and 8a). For instance, seismic profiles (SM184 to 187 [*Carton et al*., 2007], M97-15, and M99-13 [*İmren et al*., 2001]) across the Central High where the concentration of gas emissions is very dense, clearly image a highly fractured anticline, providing the fault network for fluid ascent (Figure 8a).

Based on the spatial distribution of gas seeps, it is clear that gases escaping in the Sea of Marmara and coming from different sources use migration pathways from different fault networks, namely, the MMF fault system and the inherited faults. Gas emissions documented, for instance, near the fault that borders the Tekirdağ Basin to the south are very likely produced by vertical migration along the Main Marmara Fault. Along the western margin of this same basin, however, faults in relation to the small thrust belt located there and with the Ganos uplift [*Şengör et al*., 2014] may instead provide suitable pathways for fluid migration. Basement structures may also indirectly constrain the migration pathways. Below the Central High, Çınarcık and North İmralı basins, deep seismic soundings reveal that the basement has been structured as tilted blocks, probably in the early stages of extension in the Sea of Marmara [*Laigle et al*., 2008]. The basement, relatively close to the seabed in places near the southern rim of the Çınarcık Basin, deepens southwestward, below the North Imralı Basin, and northeastward, below the Çınarcık Basin. In the North İmralı Basin, gas emissions were observed, where an array of antithetic, south dipping normal faults outcrop at the sea-bottom through recent sediments [*Laigle et al*., 2008]. Similarly, near the southern Çınarcık rim, gas emissions were found near local north dipping normal faults, which are supposedly responsible for the near-seabed basement and the deformation of recent sediments [*Laigle et al*., 2008].

Moreover, fault intersection areas constitute preferential zones for gas escapes with regard to connection with gas sources. For instance, the dense gas emissions identified in the western side of the Central basin (see around 40°49.5′N–27°56.2′E, Figure 7) are located within a zone of fault branching and interaction, between NW-SE striking normal faults and strike-slip faults with diverse (N70° to N110°) orientations.

However, the relation between seepage and fault activity is far from linear, although most of the seeps preferentially follow traces of active faults. Indeed, scarps corresponding to fault strands with unclear recent activity (e.g., North Tekirdağ, southeastern border of the Central Basin) and to inactive faults (e.g., Western High, Çınarcık Basin) continue to channel fluids. It is, however, sometimes difficult to identify cessation of fault activity with certainty. For example, the South Marmara Fault, which *Le Pichon et al*. [2014] recently mapped, is covered by Pliocene to recent sediments, yet its western continuation nucleated two $M > 6$ earthquakes. However, gas emissions may provide information on fault activity. For instance, the asymmetric distribution of gas emissions along the edges of the inner structure of the Central Basin may be related to a contrast in the recent activity of the faults [*Laigle et al*., 2008], as the southern branch of the spindle has faster recent slip rates, at least in terms of the vertical component [*Armijo et al*., 2005; *Grall et al*., 2012].

Gas seepage, as previously mentioned (Figures 4, 6, and 8), is widespread on the topographic Western and Central highs [*Grall et al*., 2013; *İmren et al*., 2001; *Thomas et al*., 2012], where fluid emission zones may also be linked with deformation zones. On the highs, acoustic gas flares appear along the main fault scarps but may also be associated with distributed deformation, expressed as folds and minor faults [*Grall*, 2013; *Şengör et al*., 2014] (Figure 6a) or, locally, with the sediment mobilization processes. The seep distribution underlines the importance of the anticline structures acting as gas traps [*Jenyon*, 1990] and of the faults that accommodate the deformation. On the Western High, gas emissions are distributed on small-scale reliefs orientated SSW-NNE and WSW-ENE along the trend of the folds and thrusts deforming the Western High [*İmren et al*., 2001] or subparallel to the MMF and are likely associated with minor strike-slip faults. In addition to the compressive structures on the Western High, the dextral strike-slip setting, involving the two branches of the NAF separated by 6 km, could certainly favor weakening of the band in between, generating fractures and faults, including normal faulting [*Thomas et al*., 2012] and clockwise block rotation, providing pathways for fluids to migrate. On the western part of the Central High (south of the Kumburgaz Basin), the East-west trending lineaments of gas emissions present on the western part of the Central High (west of 28°35′E) may be related to a series of minor strike-slip faults accommodating distributed deformation.

5.2.2. Sedimentary Control

The sedimentary control of gas emission distribution and occurrence involves the nature and thickness of the sediments and the deformation, destabilization, and erosion processes. No gas seeps have been found within the undeformed parts of the deep sedimentary basins where sediment thicknesses are important (kilometric). In the Tekirdağ Basin, for instance, only two gas emission sites were detected within the inner parts of the basin, suggesting that, wherever unfaulted, the uppermost clayey sediment layers are impermeable to gas migration. As the Thrace Basin extends offshore in the Sea of Marmara including the Tekirdağ Basin [*Görür and Elbek*, 2013; *Sen et al*., 2009], the absence of gas in the central part of the Tekirdağ basin is unlikely. The Eocene Thrace Basin including the Ganos flysch wedge extends all the way down to the Main Marmara Fault [*Le Pichon et al*., 2014] (Figure 4c). Hence, the acoustic anomalies present all along the edges of the Tekirdağ Basin could result from lateral gas migration from the center to the edges of the basin along buried, permeable silty-sandy turbidite layers and/or from vertical gas migration along subvertical faults bordering the basin. Both of these possibilities may have involved gas migration within the Eocene-Oligocene sediments of the Thrace Basin that presumably extends southward, at least to the location of the Main Marmara Fault [*Hosgormez and Yalcin*, 2005; *Le Pichon et al*., 2014] (Figure 4c). Similarly, in the eastern edge, which borders the Western High, gas could be leaking out from the Western High or be laterally transported from sources located within permeable sediment layers underlying the basin.

Very few seeps were observed in zones of highest sedimentation ($>$1 mm/yr), namely, the deep sedimentary basins [e.g., *Armijo et al*., 2005; *Çağatay et al*., 2004; *Seeber et al*., 2006; *Sorlien et al*., 2012], unless active fault scarps occur. Gas is not expelled at the seafloor unless the shallow sediments experience deformation, either resulting from tectonic faulting or from slope instability. For instance, gas seeps are observed related to the deformation (faults, folds) of the sediment cover, such as those in the Central Basin and in the Çınarcık Basin (Figures 7 and 9, respectively). Seeps are also commonly observed in relation to erosional features, such as scars of the sediment cover induced by gravity slumping or mass-transport deposits (see examples on the Western and Central highs, Figures 6b, 6c, and 8b). On the Central High, these sedimentary instabilities (Figure 8b) may be induced by gravity, fluid and seismic activity, and most likely a combination of these factors.

Thus, the absence of gas at the seabed may be explained by the sedimentary architecture and the physicochemical conditions of the sediments. Furthermore, it is worth noting that the biochemical processes occurring in the near-seabed sediments could impact on the gas fluxes. The AOM for instance could be an effective mechanism preventing upward escape of methane into the water column [*Hensen et al*., 2003; *Pohlman et al*., 2013]. The depth of AOM (methane/sulfate boundary) in the deep Marmara subbasins is at 3–4 m below the seafloor [*Çağatay et al*., 2004]. Along the southern border of the Tekirdağ Basin, the absence of acoustic gas emissions in the water column (Figures 4b and 6) along a 3 km short segment of the MMF located at the mouth of a deep sea fan-like structure could possibly be related to the AOM at depth. This view is supported by the presence of dark reduced sediment patches with bacterial mats on the seabed observed along this segment [*Zitter et al*., 2008], which are evidence of the presence of sulfur and possibly methane.

5.3. Links Between Gas Emissions and (Micro)Seismicity

Most of the seeps are located in the northern side of the Sea of Marmara in relation to the North Anatolian Fault system and, particularly but not only, with the Main Marmara Fault. Most of the gas emissions are tectonically controlled and predominately associated with active faults rather than with inactive ones.

The permanent, continuous monitoring based on land stations indicates that the microseismicity is unevenly distributed within the Sea of Marmara (Figure 4d). Swarms of microseismicity exist, most particularly in the eastern part of the Sea of Marmara (Çınarcık Basin) and in the Central Basin and Western High [*Bulut et al*., 2009; *Gurbuz et al*., 2000; *Sato et al*., 2004; H. Karabulut, personal communication, 2014], where numerous densely spaced gas emission sites are documented (Figures 4, 6a, 7, 8a, and 9). The presence of gas accumulations along the MMF across the Western High could reflect the current high level of microseismicity along the MMF, from the Ganos bend all the way to the Western High.

In contrast, the Istanbul-Silivri segment is characterized by a relative absence of microseismic activity, most particularly across the Kumburgaz Basin and the Central High. Similarly, the Princes Islands segment along the northern Çınarcık Basin corresponds to an earthquake gap [*Bohnhoff et al*., 2013]. Both of these segments record little or even no gas emissions at the seabed. Our previous work [*Géli et al*., 2008], based on limited sparse acoustic profiles, pointed out that the Istanbul-Silivri segment, which admittedly has not ruptured since 1766, was characterized by relatively fewer gas emissions compared to the adjacent segments. The systematic coverage presented here provides the possibility of refining our analysis. A closer view of the acoustic data reveals that (i) no gas emission sites are detected along the 5 km long segment connecting the Central High to the Kumburgaz Basin, as well as along the 5 km long segment at the northern border of the Çınarcık Basin, which is part of the northern Princes Islands segment; (ii) a relative smaller density of gas emissions is observed east of the segment across the Central High and along the northern border of the Kumburgaz Basin; and (iii) acoustic gas emissions may help identify the trace at the seabed of the MMF, e.g., the segment crossing the northern border of the Kumburgaz Basin.

Considering that earthquake shaking may induce degassing processes from gas prone surface layers, as a recent analysis of combined ocean bottom seismometer recordings and piezometer measurements [*Bayrakci et al*., 2014] suggested, all above observations suggest that a strong correlation exists between the occurrence of gas emissions and the present-day microseismic activity. Although the relative absence of gas emissions through the seabed into the water column, considering the presence of gas source(s) below, may be related locally to differences in sediment properties (mechanical and physicochemical) and processes (AOM), we propose that the absence of earthquake-induced ground shaking is the primary factor responsible for the relative absence of gas emissions along the Istanbul-Silivri segment and part of the Princes Islands segment. The Istanbul-Silivri segment that was thought to generate the next major earthquake in the region of Istanbul based on microseismicity [*Bohnhoff et al*., 2013] and high present-day stress there [*Pondard et al*., 2007] appears, in the light of recent works [*Ergintav et al*., 2014], to be characterized by continuous creep and, therefore, to be less problematic with regard to potential future earthquake generation. However, the Princes Islands segment appears, according to the same authors *Ergintav et al*. [2014], to be locked, making this area very dangerous with regard to geohazards in the Istanbul region.

Thus, as microseismicity gaps are, in general, where large earthquake ruptures are expected, a lack of gas emissions along these segments of the NAF may potentially indicate the locations of future seismic events. This highlights the importance of measuring long-term multiparameter time series with seafloor observatories, including gas escape monitoring [e.g., *Bayrakci et al*., 2014; *Embriaco et al*., 2014] at specific sites (i.e., along the Istanbul-Silivri and the Princes Islands segments) in order to understand the fluid emission activity with regard to the microseismicity cycle (and seismic activity), including the time lag between them.

5.4. Geological Implications at a Regional Scale

5.4.1. Relationship With the Thrace Basin: Connections With the Gas Sources

The Thrace Basin initiated as a fore-arc basin during the late Cretaceous-early Eocene, in relation to the closure of the Tethyan Ocean. It later evolved to a postcollisional basin in which the Eocene and Oligocene hydrocarbon source rocks were deposited. The NAF developed during the Middle-Late Miocene as a broad shear zone along the Intra-Pontide suture zone that formed after the subduction of the Tethyan Ocean [e.g., *Görür and Okay*, 1996; *Görür and Elbek*, 2013; *Perincek*, 1991; *Şengör et al*., 2005]. Testing the genetic relationship between onshore and offshore gases could help to better define the limit of the Thrace Basin

gas province in the Sea of Marmara [*Le Pichon et al*., 2014] (Figure 4c), in particular, in the eastern part which is less constrained. This represents a key element that could help in the understanding of the complexities of the present-day North Anatolian Fault.

Within the offshore extension of the Eocene Thrace Basin (Figure 4c), numerous closely spaced, acoustic gas anomalies were observed: on the western slope of the Tekirdağ, Central, and Kumburgaz basins, on the Western High, and on the Central High. As the hydrocarbon Eocene Thrace Basin constitutes the basement of the Sea of Marmara [*Görür and Elbek*, 2013], deep-seated faults may cut hydrocarbon traps within the basement, and gas (and oil) could naturally migrate up to the surface, seep at the seafloor, and escape into the water column, as observed. The genetic relationship between the Thrace Basin gas reservoir province and the Sea of Marmara gas emissions was clearly demonstrated in the Western High, based on the geochemical gas analysis [*Bourry et al*., 2009; *Ruffine et al*., 2012] (Figure 2). Farther east, the Central High is characterized by emissions of mainly thermogenic methane but coming from a different reservoir than the gases emitted at the Western High [*Bourry et al*., 2009]. Moreover, the biogenic methane collected at the Western and Central highs comes from the biodegradation of oil and methanogenesis, requiring a reservoir at a depth of less than 2 km, which has not yet been identified onshore (L. Ruffine, personal communication, 2014). At the Çınarcık Basin, although most of the gas, namely, methane, is clearly biogenic in origin [*Bourry et al*., 2009], a small amount of thermogenic ethane has been identified [*Bourry et al*., 2009; *Ruffine et al*., 2012] together with evidence for the occurrence of anaerobic oxidation of nonmethane hydrocarbons, including oil [*Chevalier et al*., 2011]. Although bacterial methane may be widespread at shallow levels within the Plio-Pleistocene sediments, it is most likely that a large amount of gas emissions in the Sea of Marmara, in particular, the ones localized on faults, belongs to the Eocene Thrace Basin and have, therefore, a thermogenic origin. Further geochemical investigation would be required to clearly identify the gas (and oil) source(s) and reservoirs, in particular, in the eastern part of the Sea of Marmara.

Here we hypothesize, in agreement with *Le Pichon et al*. [2014] and in accordance with geochemical data available so far, that the Eocene Thrace Basin province could be bound by the Main Marmara Fault as it crosses the Western High and the Central Basin, by the southern and eastern borders of the Central High, and possibly further east. Within this framework, it is interesting to note that the eastern border of the Thrace Basin, within the present-day Sea of Marmara, appears to coincide with the offshore continuation of the Strandja basement, as *Le Pichon et al*. [2014] indicated.

5.4.2. Relationship to the Pre-Quaternary Marmara Shear Zone and Contribution to the Understanding of the Tectonic Evolution of the Marmara Region

Gas emissions were not only found along the Main Marmara Fault Valley and on the borders of the basins. The gas escapes were also observed above some other faults reflecting the complex tectonic evolution of the Marmara Region. This underlines the importance of inherited faults in the control of gas migration from deep levels to the seabed from which gas may be expelled into the water column. The distribution of gas emissions also underlines a buried, complex fault network inherited from this history, with numerous fault strands of varying dips and strikes.

In the Western Sea of Marmara, numerous closely spaced gas emissions appear along the strike-slip structure, subparallel to the MMF, delineating the Western High to the north, all the way eastward to the base of the northern escarpment of the Central Basin. The Western High represents a middle Miocene structure cut by younger strike-slip faults [*Görür and Elbek*, 2013]. The general picture of the distribution of acoustic anomalies suggests the hypothesis that the gas emissions trends underline the tectonic faults that were active during the late Pliocene to Pleistocene [*Görür and Elbek*, 2013], in relation to the focusing of the deformation along the present-day Main Marmara Fault, as argued by *Şengör et al*. [2005]. The Western High appears, therefore, to have recently evolved between two right-lateral strike-slip faults and experienced shear deformation, along with clockwise rotation.

6. Conclusions

Gas seeps in the Sea of Marmara, although partly and locally constrained by the nature and thickness of the sedimentary cover, are clearly controlled by the fault and fracture networks. The connection to the gas sources undoubtedly involves the underlying Eocene Thrace Basin, a well-known and prolific gas province,

as evidenced by the geochemical signature of collected gases in the western part of the Sea of Marmara. Gas analyses of samples collected farther east could help to better define the offshore and eastern extent of the Thrace Basin by establishing the nature and origin of the gases and their possible genetic link to the known onshore petroleum system and offshore underlying reservoirs.

Although gas emissions may be associated to inactive fault segments, they are on the most part associated with active fault segments. The gas emission sites are thus mainly concentrated in the northern part of the Sea of Marmara where the northern branch of the North Anatolian Fault lies, in particular, in connection with but not only the Main Marmara Fault. The inherited fault network, besides the MMF fault system, plays a role in controlling the migration and distribution of the gases.

We observe a strong correlation between the occurrence of gas emissions and present-day microseismic activity. Gas emissions are located along most of the MMF, with the exception of a few 5 km long segments, one located along the southern border of the Tekirdağ Basin and two others which are part of the Istanbul-Silivri and Princes Islands segments. Whereas sedimentary loading and biogeochemical processes in the near surface may have explained the absence of gas emissions along the southern Tekirdağ segment, the absence of earthquake-induced ground shaking along the two other segments is most likely the primary factor responsible for the relative absence of gas emissions there. The Princes Islands segment, moreover, appears to be locked according to *Ergintav et al.* [2014], making this area very dangerous in regard to geohazards.

The gas emission activity appears persistent through time; however, evidence for temporal variations of local sources was also documented over a broad range of time scales (minutes to years). In this context, studying the spatiotemporal activity of gas emissions is a difficult challenge. Significant effort must be made to focus multidisciplinary studies on selected segments along the North Anatolian Fault, for instance, the Princes Islands segment, where monitoring of gas seeps may provide insights on the occurrence of seismic events. Through repeated acoustic measurements, valuable information may be obtained on fluid migration upon ground shaking at this specific location, which is close to Istanbul, one of the largest inhabited regions threatened by earthquakes and tsunamis.

Acknowledgments

We would like to thank the captain and crew of R/V *Le Suroît*, as well as the scientific party of the Marmesonet expedition. We also greatly acknowledge the support of the Turkish Navy, who largely contributed to the success of the expedition in the heavily navigated Marmara Sea. We would like to offer our gratitude to Charline Guérin, Hélène Clouet, and André Ogor for their contribution in the processing of the acoustic water column data. Hayrullah Karabulut and Jean Schmittbuhl provided unpublished maps of relocated microseismicity that were very useful for our interpretation. The Marmesonet expedition was part of the Marmara Demonstration Mission project within the ESONET Network of Excellence (NoE), cofunded by the European Commission in the Framework Programme FP6. Data interpretation work was funded in part by the MARSITE European Commission FP7 project. The data for this paper are available at the French National Oceanographic Data Centre, SISMER. http://www.ifremer.fr/sismerData/jsp/visualisationMetadata2.jsp?strPortail=ifremer&langue=EN&pageOrigine=CAM&cle1=FI352009020040. We are grateful to Christian Berndt and an anonymous reviewer for their constructive comments that substantially improved the manuscript.

References

Aksoy, M. E., M. Meghraoui, M. Vallée, and Z. Çakır (2010), Rupture characteristics of the A.D. 1912 Mürefte (Ganos) earthquake segment of the North Anatolian fault (western Turkey), *Geology*, *38*(11), 991–994, doi:10.1130/g31447.1.

Alpar, B. (1999), Underwater signatures of the Kocaeli eartquake of 17 August 1999 in Turkey, *Turk. J. Mar. Sci.*, *5*, 111–130.

Ambraseys, N. N., and C. F. Finkel (1987), The Saros Marmara earthquake of 9 August 1912, *Earthquake Eng. Struct. Dynam.*, *15*(2), 189–211, doi:10.1002/eqe.4290150204.

Ambraseys, N. N., and J. A. Jackson (2000), Seismicity of the Sea of Marmara (Turkey) since 1500, *Geophys. J. Int.*, *141*(3), F1–F6.

Armijo, R., B. Meyer, A. Hubert, and A. Barka (1999), Westward propagation of the North Anatolian fault into the northern Aegean: Timing and kinematics, *Geology*, *27*(3), 267–270, doi:10.1130/0091-7613(1999)027<0267:wpotna>2.3.co;2.

Armijo, R., B. Meyer, S. Navarro, G. King, and A. Barka (2002), Asymmetric slip partitioning in the Sea of Marmara pull-apart: A clue to propagation processes of the North Anatolian Fault?, *Terra Nova*, *14*(2), 80–86, doi:10.1046/j.1365-3121.2002.00397.x.

Armijo, R., et al. (2005), Submarine fault scarps in the Sea of Marmara pull-apart (North Anatolian Fault): Implications for seismic hazard in Istanbul, *Geochem. Geophys. Geosyst.*, *6*, Q06009, doi:10.1029/2004GC000896.

Augustin, J.-M. (2011), Developing and deploying sonar and echosounder data analysis software, *Matlab Newsletters*. [Available at http://www.mathworks.fr/company/newsletters/articles/developing-and-deploying-sonar-and-echosounder-data-analysis-software.html.]

Barka, A., et al. (2002), The surface rupture and slip distribution of the 17 August 1999 Izmit earthquake (*M* 7.4), North Anatolian fault, *Bull. Seismol. Soc. Am.*, *92*(1), 43–60, doi:10.1785/0120000841.

Bayrakci, G., et al. (2014), Acoustic monitoring of gas emissions from the seafloor. Part II: A case study from the Sea of Marmara, *Mar. Geophys. Res.*, 1–19, doi:10.1007/s11001-014-9227-7.

Bécel, A., M. Laigle, B. de Voogd, A. Hirn, T. Taymaz, S. Yolsal-Cevikbilen, and H. Shimamura (2010), North Marmara Trough architecture of basin infill, basement and faults, from PSDM reflection and OBS refraction seismics, *Tectonophysics*, *490*(1–2), 1–14, doi:10.1016/j.tecto.2010.04.004.

Bohnhoff, M., F. Bulut, G. Dresen, P. E. Malin, T. Eken, and M. Aktar (2013), An earthquake gap south of Istanbul, *Nat. Commun.*, *4*, doi:10.1038/ncomms2999.

Bourry, C., B. Chazallon, J. L. Charlou, J. Pierre Donval, L. Ruffine, P. Henry, L. Geli, M. N. Çagatay, S. Inan, and M. Moreau (2009), Free gas and gas hydrates from the Sea of Marmara, Turkey: Chemical and structural characterization, *Chem. Geol.*, *264*(1–4), 197–206, doi:10.1016/j.chemgeo.2009.03.007.

Bulut, F., M. Bohnhoff, W. L. Ellsworth, M. Aktar, and G. Dresen (2009), Microseismicity at the North Anatolian Fault in the Sea of Marmara offshore Istanbul, NW Turkey, *J. Geophys. Res.*, *114*, B09302, doi:10.1029/2008JB006244.

Çağatay, M. N., M. Ozcan, and E. Gungor (2004), Pore-water and sediment geochemistry in the Marmara Sea (Turkey): Early diagenesis and diffusive fluxes, *Geochem. Explor. Environ. Anal.*, *4*, 213–225, doi:10.1144/1467-7873/04-202.

Capozzi, R., and V. Picotti (2002), Fluid migration and origin of a mud volcano in the Northern Apennines (Italy): The role of deeply rooted normal faults, *Terra Nova*, *14*(5), 363–370, doi:10.1046/j.1365-3121.2002.00430.x.

Carton, H., et al. (2007), Seismic imaging of the three-dimensional architecture of the Çınarcık Basin along the North Anatolian Fault, *J. Geophys. Res.*, *112*, B06101, doi:10.1029/2006JB004548.

Chevalier, N., I. Bouloubassi, D. Birgel, A. Crémière, M.-H. Taphanel, and C. Pierre (2011), Authigenic carbonates at cold seeps in the Marmara Sea (Turkey): A lipid biomarker and stable carbon and oxygen isotope investigation, *Mar. Geol.*, *288*(1–4), 112–121, doi:10.1016/j.margeo.2011.08.005.

Christodoulou, D., G. Papatheodorou, G. Ferentinos, and M. Masson (2003), Active seepage in two contrasting pockmark fields in the Patras and Corinth gulfs, Greece, *Geo Mar. Lett.*, *23*(3–4), 194–199, doi:10.1007/s00367-003-0151-0.

Cormier, M. H., et al. (2006), North Anatolian Fault in the Gulf of Izmit (Turkey): Rapid vertical motion in response to minor bends of a nonvertical continental transform, *J. Geophys. Res.*, *111*, B04102, doi:10.1029/2005JB003633.

Crémière, A., C. Pierre, M.-M. Blanc-Valleron, T. Zitter, M. N. Çağatay, and P. Henry (2012), Methane-derived authigenic carbonates along the North Anatolian fault system in the Sea of Marmara (Turkey), *Deep Sea Res., Part I*, *66*, 114–130, doi:10.1016/j.dsr.2012.03.014.

Delisle, G., U. von Rad, H. Andruleit, C. H. von Daniels, A. R. Tabrez, and A. Inam (2002), Active mud volcanoes on- and offshore eastern Makran, Pakistan, *Int. J. Earth Sci.*, *91*(1), 93–110, doi:10.1007/s005310100203.

Deville, E., A. Mascle, S. H. Guerlais, C. Decalf, and B. Colletta (2003), Lateral changes of frontal accretion and mud volcanism processes in the Barbados accretionary prism and some implications, The Circum-Gulf of Mexico and the Caribbean: Hydrocarbon habitats, basin formation, and plate tectonics, *AAPG Mem*., 79, 656-674.

Dewey, J. F., and A. M. C. Şengör (1979), Aegean and surrounding regions: complex multi-plate and continuum tectonics in a convergent zone, *Geol. Soc. Am. Bull.*, *90*(1), 84–92, doi:10.1130/0016-7606(1979)90<84:aasrcm>2.0.co;2.

Dragesund, O., and S. Olsen (1965), On the possibility of estimating year-class strength by measuring echo-abundance of 0-group fish, *Fiskeridir. Skrifter Ser. Havunders.*, *13*(8), 48–65.

Dumke, I., I. Klaucke, C. Berndt, and J. Bialas (2014), Sidescan backscatter variations of cold seeps on the Hikurangi Margin (New Zealand): indications for different stages in seep development, *Geo Mar. Lett.*, *34*(2–3), 169–184, doi:10.1007/s00367-014-0361-7.

Dupré, S., J. Woodside, I. Klaucke, J. Mascle, and J.-P. Foucher (2010), Widespread active seepage activity on the Nile Deep Sea Fan (offshore Egypt) revealed by high-definition geophysical imagery, *Mar. Geol.*, *275*(1–4), 1–19, doi:10.1016/j.margeo.2010.04.003.

Dupré, S., L. Berger, N. Le Bouffant, C. Scalabrin, and J.-F. Bourillet (2014a), Fluid emissions at the Aquitaine Shelf (Bay of Biscay, France): A biogenic origin or the expression of hydrocarbon leakage?, *Cont. Shelf Res.*, *88*, 24–33, doi:10.1016/j.csr.2014.07.004.

Dupré, S., J. Mascle, J.-P. Foucher, F. Harmegnies, J. Woodside, and C. Pierre (2014b), Warm brine lakes in craters of active mud volcanoes, Menes caldera off NW Egypt: Evidence for deep-rooted thermogenic processes, *Geo Mar. Lett.*, *34*(2–3), 153–168, doi:10.1007/s00367-014-0367-1.

Embriaco, D., et al. (2014), Monitoring of gas and seismic energy release by multiparametric benthic observatory along the North Anatolian Fault in the Sea of Marmara (NW Turkey), *Geophys. J. Int.*, *196*(2), 850–866, doi:10.1093/gji/ggt436.

Ergintav, S., R. E. Reilinger, R. Çakmak, M. Floyd, Z. Cakir, U. Doğan, R. W. King, S. McClusky, and H. Özener (2014), Istanbul's earthquake hot spots: Geodetic constraints on strain accumulation along faults in the Marmara seismic gap, *Geophys. Res. Lett.*, *41*, 5783–5788, doi:10.1002/2014gl060985.

Field, M. E., and A. E. Jennings (1987), Seafloor gas seeps triggered by a northern California earthquake, *Mar. Geol.*, *77*(1–2), 39–51, doi:10.1016/0025-3227(87)90082-x.

Foucher, J. P., S. Dupré, C. Scalabrin, T. Feseker, F. Harmegnies, and H. Nouzé (2010), Changes in seabed morphology, mud temperature and free gas venting at the Håkon Mosby Mud Volcano, offshore Northern Norway, over the time period 2003–2006, *Geo Mar. Lett.*, *30*, 157–167, doi:10.1007/s00367-010-0193-z.

Gasperini, L., A. Polonia, F. Del Bianco, P. Favali, G. Marinaro, and G. Etiope (2012), Cold seeps, active faults and the earthquake cycle along the North Anatolian Fault system in the Sea of Marmara (NW Turkey), *Boll. Geofis. Teor. Appl.*, *53*(4), 371–384, doi:10.4330/bgta0082.

Gay, A., M. Lopez, C. Berndt, and M. Séranne (2007), Geological controls on focused fluid flow associated with seafloor seeps in the Lower Congo Basin, *Mar. Geol.*, *244*(1–4), 68–92, doi:10.1016/j.margeo.2007.06.003.

Géli, L., et al. (2008), Gas emissions and active tectonics within the submerged section of the North Anatolian Fault zone in the Sea of Marmara, *Earth Planet. Sci. Lett.*, *274*, 34–39, doi:10.1016/j.epsl.2008.06.047.

Görür, N., and S. Elbek (2013), Tectonic events responsible for shaping the Sea of Marmara and its surrounding region, *Geodin. Acta*, *26*(1–2), 1–11, doi:10.1080/09853111.2013.859346.

Görür, N., and A. I. Okay (1996), A fore-arc origin for the Thrace Basin, NW Turkey, *Geologische Rundschau*, *85*(4), 662–668, doi:10.1007/bf02440103.

Grall, C. (2013), La Faille Nord Anatolienne dans sa portion immergée en mer de Marmara: Evolution du réseau de failles et migration de fluides, Thèse de doctorat d'Aix-Marseille Université.

Grall, C., P. Henry, D. Tezcan, B. Mercier de Lepinay, A. Bécel, L. Géli, J.-L. Rudkiewicz, T. Zitter, and F. Harmegnies (2012), Heat flow in the Sea of Marmara Central Basin: Possible implications for the tectonic evolution of the North Anatolian fault, *Geology*, doi:10.1130/g32192.1.

Grall, C., P. Henry, Y. Thomas, G. K. Westbrook, M. N. Çağatay, B. Marsset, H. Saritas, G. Çifçi, and L. Géli (2013), Slip rate estimation along the western segment of the Main Marmara Fault over the last 405–490 ka by correlating mass transport deposits, *Tectonics*, *32*, 1587–1601, doi:10.1002/2012tc003255.

Gurbuz, C., et al. (2000), The seismotectonics of the Marmara region (Turkey): Results from a microseismic experiment, *Tectonophysics*, *316*(1–2), 1–17, doi:10.1016/s0040-1951(99)00253-x.

Hasiotis, T., G. Papatheodorou, N. Kastanos, and G. Ferentinos (1996), A pockmark field in the Patras Gulf (Greece) and its activation during the 14/7/93 seismic event, *Mar. Geol.*, *130*(3–4), 333–344, doi:10.1016/0025-3227(95)00131-x.

Henry, P., S. Lallemant, K.-I. Nakamura, U. Tsunogai, S. Mazzotti, and K. Kobayashi (2002), Surface expression of fluid venting at the toe of the Nankai wedge and implications for flow paths, *Mar. Geol.*, *187*(1–2), 119–143, doi:10.1016/S0025-3227(02)00262-1.

Hensen, C., M. Zabel, K. Pfeifer, T. Schwenk, S. Kasten, N. Riedinger, H. D. Schulz, and A. Boettius (2003), Control of sulfate pore-water profiles by sedimentary events and the significance of anaerobic oxidation of methane for the burial of sulfur in marine sediments, *Geochim. Cosmochim. Acta*, *67*(14), 2631–2647, doi:10.1016/s0016-7037(03)00199-6.

Hosgormez, H., and M. N. Yalcin (2005), Gas-source rock correlation in Thrace basin, Turkey, *Mar. Pet. Geol.*, *22*(8), 901–916, doi:10.1016/j.marpetgeo.2005.04.002.

İmren, C., X. Le Pichon, C. Rangin, E. Demirbağ, B. Ecevitoğlu, and N. Görür (2001), The North Anatolian Fault within the Sea of Marmara: A new interpretation based on multi-channel seismic and multi-beam bathymetry data, *Earth Planet. Sci. Lett.*, *186*(2), 143–158, doi:10.1016/s0012-821x(01)00241-2.

Jenyon, M. K. (1990), *Oil and Gas Traps: Aspects of their Seismostratigraphy, Morphology, and Development*, vol. 398, Wiley, Chichester, U. K.

Judd, A. G., and M. Hovland (2007), *Seabed Fluid Flow. The Impact on Geology, Biology and the Marine Environment*, pp. 293, Cambridge Univ. Press, Cambridge, U. K.

Karabulut, H., J. Schmittbuhl, S. Ozalaybey, O. Lengline, A. Komec-Mutlu, V. Durand, M. Bouchon, G. Daniel, and M. P. Bouin (2011), Evolution of the seismicity in the eastern Marmara Sea a decade before and after the 17 August 1999 Izmit earthquake, *Tectonophysics*, *510*(1–2), 17–27, doi:10.1016/j.tecto.2011.07.009.

Ketin, I. (1948), Über die tektonisch-mechanischen Folgerungen aus den großen anatolischen Erdbeben des letzten Dezenniums, *Geol. Rundsch.*, *36*(1), 77–83, doi:10.1007/bf01791916.

Kopf, A. J. (2002), Significance of mud volcanism, *Rev. Geophys.*, *40*(2), 1005, doi:10.1029/2000RG000093.

Kusçu, I., M. Okamura, H. Matsuoka, E. Gökasan, Y. Awata, H. Tur, M. Simsek, and M. Keçer (2005), Seafloor gas seeps and sediment failures triggered by the August 17, 1999 earthquake in the Eastern part of the Gulf of Izmit, Sea of Marmara, NW Turkey, *Mar. Geol.*, *215*(3–4), 193–214, doi:10.1016/j.margeo.2004.12.002.

Laigle, M., A. Becel, B. de Voogd, A. Hirn, T. Taymaz, and S. Ozalaybey (2008), A first deep seismic survey in the Sea of Marmara: Deep basins and whole crust architecture and evolution, *Earth Planet. Sci. Lett.*, *270*(3–4), 168–179, doi:10.1016/j.epsl.2008.02.031.

Le Pichon, X., K. Kobayashi, and C. Kaiko-Nankai Scientific (1992), Fluid venting activity within the eastern Nankai trough accretionary wedge: A summary of the 1989 Kaiko-Nankai results, *Earth Planet. Sci. Lett.*, *109*(3–4), 303–318, doi:10.1016/0012-821X(92)90094-C.

Le Pichon, X., et al. (2001), The active Main Marmara Fault, *Earth Planet. Sci. Lett.*, *192*(4), 595–616, doi:10.1016/s0012-821x(01)00449-6.

Le Pichon, X., C. İmren, C. Rangin, A. M. C. Şengör, and M. Siyako (2014), The South Marmara Fault, *Int. J. Earth Sci.*, *103*(1), 219–231, doi:10.1007/s00531-013-0950-0.

Loncke, L., J. Mascle, and P. Fanil Scientific (2004), Mud volcanoes, gas chimneys, pockmarks and mounds in the Nile deep-sea fan (Eastern Mediterranean): Geophysical evidences, *Mar. Pet. Geol.*, *21*(6), 669–689, doi:10.1016/j.marpetgeo.2004.02.004.

McClusky, S., et al. (2000), Global Positioning System constraints on plate kinematics and dynamics in the eastern Mediterranean and Caucasus, *J. Geophys. Res.*, *105*(B3), 5695–5719, doi:10.1029/1999JB900351.

Mellors, R., D. Kilb, A. Aliyev, A. Gasanov, and G. Yetirmishli (2007), Correlations between earthquakes and large mud volcano eruptions, *J. Geophys. Res.*, *112*, B04304, doi:10.1029/2006JB004489.

Merewether, R., M. S. Olsson, and P. Lonsdale (1985), Acoustically detected hydrocarbon plumes rising from 2-km depths in Guaymas Basin, Gulf of California, *J. Geophys. Res.*, *90*(B4), 3075–3085, doi:10.1029/JB090iB04p03075.

Moore, J. C., D. Orange, and L. D. Kulm (1990), Interrelationship of fluid venting and structural evolution: Alvin observations from the frontal accretionary prism, Oregon, *J. Geophys. Res.*, *95*(B6), 8795–8808, doi:10.1029/JB095iB06p08795.

Okay, A. I., E. Demirbag, H. Kurt, N. Okay, and I. Kuscu (1999), An active, deep marine strike-slip basin along the North Anatolian fault in Turkey, *Tectonics*, *18*(1), 129–147, doi:10.1029/1998TC900017.

Parke, M., W. Anderson, K. McKenzie, G. Bull, and C. Şengör (1999), Active faults in the Sea of Marmara, western Turkey, imaged by seismic reflection profiles, *Terra Nova*, *11*(5), 223–227, doi:10.1046/j.1365-3121.1999.00248.x.

Parke, R. S. White, D. McKenzie, T. A. Minshull, J. M. Bull, I. Kusçu, N. Görür, and C. Sengör (2002), Interaction between faulting and sedimentation in the Sea of Marmara, western Turkey, *J. Geophys. Res.*, *107*(B11), 2286, doi:10.1029/2001JB000450.

Paull, C. K., W. Ussler III, W. S. Borowski, and F. N. Spiess (1995), Methane-rich plumes on the Carolina continental rise: Associations with gas hydrates, *Geology*, *23*(1), 89–92.

Perincek, D. (1991), Possible strand of the North Anatolian Dault in the Thrace Basin, Turkey - An interpretation, *Am. Assoc. Pet. Geol. Bull.*, *75*(2), 241–257.

Pohlman, J. W., M. Riedel, J. E. Bauer, E. A. Canuel, C. K. Paull, L. Lapham, K. S. Grabowski, R. B. Coffin, and G. D. Spence (2013), Anaerobic methane oxidation in low-organic content methane seep sediments, *Geochim. Cosmochim. Acta*, *108*, 184–201, doi:10.1016/j.gca.2013.01.022.

Pondard, N., R. Armijo, G. C. P. King, B. Meyer, and F. Flerit (2007), Fault interactions in the Sea of Marmara pull-apart (North Anatolian Fault): Earthquake clustering and propagating earthquake sequences, *Geophys. J. Int.*, *171*(3), 1185–1197.

Rangin, C., E. Demirbag, C. Imren, A. Crusson, A. Normand, E. Le Drezen, and A. Le Bot (2001), *Marine Atlas of the Sea of Marmara (Turkey)*, Ifremer, Plouzané, France.

Rangin, C., X. Le Pichon, E. Demirbag, and C. Imren (2004), Strain localization in the Sea of Marmara: Propagation of the North Anatolian Fault in a now inactive pull-apart, *Tectonics*, *23*, TC2014, doi:10.1029/2002TC001437.

Reilinger, R. E., S. C. McClusky, M. B. Oral, R. W. King, M. N. Toksoz, A. A. Barka, I. Kinik, O. Lenk, and I. Sanli (1997), Global Positioning System measurements of present-day crustal movements in the Arabia-Africa-Eurasia plate collision zone, *J. Geophys. Res.*, *102*(B5), 9983–9999, doi:10.1029/96JB03736.

Rudolph, M. L., and M. Manga (2010), Mud volcano response to the 4 April 2010 El Mayor-Cucapah earthquake, *J. Geophys. Res.*, *115*, B12211, doi:10.1029/2010JB007737.

Ruffine, L., et al. (2012), Geochemical dynamics of the natural-gas hydrate system in the Sea of Marmara, offshore Turkey, in *Geochemical Dynamics of the Natural-Gas Hydrate System in the Sea of Marmara, Offshore Turkey*, Advances in Natural Gas Technology, edited by H. Al-Megren, pp. 29–56, InTech.

Sato, T., J. Kasahara, T. Taymaz, M. Ito, A. Kamimura, T. Hayakawa, and O. Tan (2004), A study of microearthquake seismicity and focal mechanisms within the Sea of Marmara (NW Turkey) using ocean bottom seismometers (OBSs), *Tectonophysics*, *391*(1–4), 303–314, doi:10.1016/j.tecto.2004.07.018.

Seeber, L., M.-H. Cormier, C. McHugh, O. Emre, A. Polonia, and C. Sorlien (2006), Rapid subsidence and sedimentation from oblique slip near a bend on the North Anatolian transform fault in the Marmara Sea, Turkey, *Geology*, *34*(11), 933–936, doi:10.1130/g22520a.1.

Sen, S., S. Yillar, and I. Erdal Kerey (2009), Allochthonous blocks misidentified as the basement: Implication for petroleum exploration in the SW Thrace Basin (Turkey), *J. Petrol. Sci. Eng.*, *64*(1–4), 55–66.

Şengör, A. M. C., O. Tuysuz, C. Imren, M. Sakinc, H. Eyidogan, G. Görür, X. Le Pichon, and C. Rangin (2005), The North Anatolian Fault: A new look, *Annu. Rev. Earth Planet. Sci.*, *33*, 37–112, doi:10.1146/annurev.earth.32.101802.120415.

Şengör, A. M. C., C. Grall, C. Imren, X. Le Pichon, N. Gorur, P. Henry, H. Karabulut, and M. Siyako (2014), The geometry of the North Anatolian transform fault in the Sea of Marmara and its temporal evolution: Implications for the development of intracontinental transform faults, *Can. J. Earth Sci.*, *51*(3), 222–242, doi:10.1139/cjes-2013-0160.

Shillington, D. J., et al. (2012), Evidence for widespread creep on the flanks of the Sea of Marmara transform basin from marine geophysical data, *Geology*, *40*(5), 439–442, doi:10.1130/g32652.1.

Sorlien, C. C., et al. (2012), Uniform basin growth over the last 500 ka, North Anatolian Fault, Marmara Sea, Turkey, *Tectonophysics*, *518–521*, 1–16, doi:10.1016/j.tecto.2011.10.006.

Soter, S. (1999), Macroscopic seismic anomalies and submarine pockmarks in the Corinth-Patras rift, Greece, *Tectonophysics*, *308*(1–2), 275–290, doi:10.1016/S0040-1951(99)00090-6.

Tary, J. B., L. Géli, C. Guennou, P. Henry, N. Sultan, N. Çağatay, and V. Vidal (2012), Microevents produced by gas migration and expulsion at the seabed: A study based on sea bottom recordings from the Sea of Marmara, *Geophys. J. Int.*, *190*(2), 993–1007, doi:10.1111/j.1365-246X.2012.05533.x.

Thomas, Y., B. Marsset, G. K. Westbrook, C. Grall, L. Géli, P. Henry, G. Cifci, A. Rochat, and H. Saritas (2012), Contribution of high-resolution 3D seismic near-seafloor imaging to reservoir-scale studies: Application to the active North Anatolian Fault, Sea of Marmara, *Near Surf. Geophys.*, *10*, 291–301, doi:10.3997/1873-0604.2012019.

Tryon, M. D., P. Henry, and D. R. Hilton (2012), Quantifying submarine fluid seep activity along the North Anatolian Fault Zone in the Sea of Marmara, *Mar. Geol.*, *315–318*, 15–28, doi:10.1016/j.margeo.2012.05.004.

Tsunogai, U., K. Maegawa, S. Sato, D. D. Komatsu, F. Nakagawa, T. Toki, and J. Ashi (2012), Coseimic massive methane release from a submarine mud volcano, *Earth Planet. Sci. Lett.*, *341–344*, 79–85, doi:10.1016/j.epsl.2012.06.004.

Zitter, T. A. C., C. Huguen, J. ten Veen, and J. M. Woodside (2006), Tectonic control on mud volcanoes and fluid seeps in the Anaximander Mountains, eastern Mediterranean Sea, *Geol. Soc. Am. Spec. Pap.*, *409*, 615–631, doi:10.1130/2006.2409(28).

Zitter, T. A. C., et al. (2008), Cold seeps along the main Marmara Fault in the Sea of Marmara (Turkey), *Deep Sea Res., Part I*, *55*(4), 552–570, doi:10.1016/j.dsr.2008.01.002.

Zitter, T. A. C., C. Grall, P. Henry, M. S. Özeren, M. N. Çağatay, A. M. C. Şengör, L. Gasperini, B. M. de Lépinay, and L. Géli (2012), Distribution, morphology and triggers of submarine mass wasting in the Sea of Marmara, *Mar. Geol.*, *329–331*, 58–74, doi:10.1016/j.margeo.2012.09.002.